群馬大学博士論文

ANALYSIS OF ELECTRONIC TRANSPORT IN SILICENE FOR SPINTRONICS

2017年9月

群馬大学大学院理工学府

知能機械創製理工学領域

Peerasak Chantngarm

Abstract

Scientists have found that we may control the spin of electrons and utilize it in spintronics, which may provide the possibility to overcome the limitation in Moore's law. Based on similar idea, valleytronics using valley degree of freedom has been proposed, and more recently pseudospintronics using pseudospin degree of freedom has also been proposed. Spintronic, valleytronic, and pseudospintronic devices are perfect candidates for quantum computers which are expected to be much faster than classical computers. On the other hand, elemental two-dimensional materials are anticipated to play an important role in spintronics, valleytronics, and pseudospintronics. They are also called Dirac materials because their electrons behave like massless Dirac particles obeying Dirac equation instead of Schrodinger equation like the electrons in other materials. One common characteristic of elemental 2D materials is the possession of honeycomb lattice structure which results in the existence of two atoms in one unit cell, and gives rise to two sublattices, A and B. This two-sublattice system contributes to a new concept called pseudospin.

Silicene is single-layer silicon. It is a relatively new elemental two-dimensional Dirac material. The main differences of silicene from graphene are the out-of-plane buckling and the larger spin-orbit interaction that allow the band gap in silicene to be tunable by electric field. The differences also cause silicene under a certain condition to behave as a topological insulator, a group of materials that have many exotic characteristics such as quantum spin Hall effect. Combining these properties with the accumulated knowledge in silicon industry makes silicene a material with great potential for spintronic and quantum computational applications.

The aim of this dissertation is to investigate the electronic transport properties of silicene for spintronics, and particularly explore the potential of silicene as a material for light sensitive devices. The dual ferromagnetic-gated silicene junction is used as the basic structure in our investigation which are separated into two parts. First, we study the electronic transport properties of the

structure to see the effects of electric field, magnetic exchange field configuration, and chemical potential on the spin-polarized, valley-polarized, and pseudospin-polarized currents. The electric fields and magnetic exchange fields are applied to ferromagnetic gates, while chemical potentials are applied to ferromagnetic gates and the normal region between gates. Second, we investigate the effects of off-resonant circularly polarized photo irradiation onto the normal region between gates under the influence of electric fields, magnetic exchange fields, and chemical potentials.

We discovered that magnetic exchange field configuration has a significant impact in the spin, valley, and pseudospin currents, and allows the device structure to behave as a pure spin polarizer, pure valley polarizer, or a pseudospin polarizer. The junction in our study exhibits perfect spin-valley polarization in certain exchange field configurations when chemical potential is applied. We also found that the peaks splitting effect on conductance is enhanced in all exchange field configurations when a middle gate bias is applied. We also predict that the pseudospin polarization can be linearly controlled by electric field from   to   when an appropriate middle gate bias is applied. This perfectly controllable pseudospin current in silicene was found only in dual ferromagnetic-gated junctions, and is not achievable with single ferromagnetic-gated junctions.

In the second part, it is found that all components of the polarized spin-valley currents in all exchange field configurations are affected by the light irradiation, probably due to the photon dressing effect. It is interesting to see possibility of spin-valley filtering when appropriate electric fields are applied to anti-parallel junctions under the light irradiation, where we can select specific spin-valley polarization to be filtered. We discovered that by adjusting the distance between two ferromagnetic gates, the light frequency for the appearance of spin-valley polarization peak can be controlled. Our investigation also revealed a possibility to control tunneling magnetoresistance (TMR) to become giant magnetoresistance (GMR) with appropriate application of electric fields and gate-induced chemical potentials under a specific light frequency. It is found that TMR magnitude may change significantly at a specific light frequency when the strength of electric field or chemical potential reaches a certain level.

Table of Contents

Chapter 1

Introduction

Cannonlake, Intel's codename for the 10nm microprocessor, is expected to be released this year. However, it is considered very hard to go beyond that, even though the theoretical scaling limit is considered to be 3 nm [1-2]. After the first observation of Moore's law by Gordon Moore in 1965 that the number of transistors in an integrated circuit will double every two years [3], now it seems to be more difficult and not economically desirable to further shrink the transistors in integrated circuits by early 2020s [4]. In the past years, scientists and engineers have worked hard to keep the Moore's law by developing new device structures and materials. The current device structure of MOSFET is far away from the original one. While the concept of controlling the drain current with gate voltage stays the same, present MOSFETs use several non-planar structures such as fin field effect transistor (finFET), gate-all-around (GAA) MOSFET, and tri-gate transistor [5-7]. Another approach that scientists and engineers also utilize in support of scaling devices is using new materials. Silicon-on-insulator (SOI), silicon germanium (SiGe), strained silicon, and high-k dielectrics are among the technologies being used widely in current MOSFETs [8-10].

At the same time, there is no doubt that electronic devices will be literally everywhere in the near future. The rise of artificial intelligence (AI) and internet of things (IoT), which is extended further into internet of everything (IoE), would materialize ubiquitous computing powered by many kinds of basic electronic devices from complementary metal–oxide–semiconductors (CMOS) to microelectromechanical systems (MEMS), and from laser diodes to photovoltaic cells. To achieve ubiquitous computing, the basic devices need to be small while being powerful enough at the same time. However, the dead end on the roadmap of miniaturization in the current semiconductor technologies causes tremendous

challenges, especially for the system that needs high computing power such as microprocessor. One possible solution is to move further into the realm of quantum mechanics. The rest of this introduction is organized as follows. In Section 1.1, we give an overview of spintronics as well as introduce the concept of valleytronics and pseudospintronics. Introduction of Dirac materials, which is the group of materials where graphene and silicene belong to, is provided in Section 1.2. We give the overview of this dissertation in Section 1.3.

1.1 From Electronics to Spintronics

Richard Feynman has mentioned about manipulating and controlling things on a small scale in 1959. Since then, the concept of nanotechnology has not been developed only in physics, but also in other fields such as chemistry and biology. When the size of a system decreases into smaller than 100 nm, the system is dictated by quantum mechanics rather than Newtonian mechanics causing quantum effects to become significant. Looking deeper into quantum mechanics, scientists found that instead of controlling electronic charges, we can also control the spin of electrons. Applications of the concept in electronic devices result in a new field called spintronics, which provides the possibility of new types of devices, and eventually the possibility to overcome the challenge facing us by going beyond the Moore's law.

Electron is an elementary particle carrying negative elementary electric charge and intrinsic angular momentum called spin with a half-integer value. From the past, electronic industry has used the charge degree of freedom of electrons. In other words, we have focused on whether there are charges, ie electrons, or not to store information and control basic devices. On the other hand, electron's spin degree of freedom is used to control spintronics devices. In spintronics, spin-up current is considered separately from spin-down current. Comparing with the conventional electronics, spintronics provides higher computing speed with lower power consumption [11].

Although quantum effects were investigated for electronic applications for a long time, we have still been in the realm of electronics using charge degree of freedom of electrons to store and process information. Quantum mechanics allows

us to go beyond electronics into the realm of spintronics, where spin degree of freedom of electrons is used. One major spintronic application is in the field of data storage. For many years, magnetic tunnel junctions (MTJ) made from metallic ferromagnetic materials have been used for read-heads of hard disk drives. Another widely used spintronic device is magnetoresistive random-access memory (MRAM). Figure 1-1 shows the schematic diagram of spin-dependent current and charge current. When electrons move, they causes flow of charge current. However, when those electrons are separated into two groups according to their polarized spin direction, we can separate the charge current into spin-up current and spin-down current.

One obstacle for more applications of spintronic devices is the necessity of magnetic field to manipulate the spin direction. However, with the recent advance in spintronic devices made from semiconductor materials instead of magnetic materials, spintronics is expected to be utilized more wildly. This is because the spin-orbit interaction in semiconductor allows the manipulation of spin states solely via electric fields and removes the requirement of magnetic field [12]. Recently, new two-dimensional materials, such as stanene (Sn) and plumbene (Pb), have attracted attention due to their larger spin-orbit interaction.
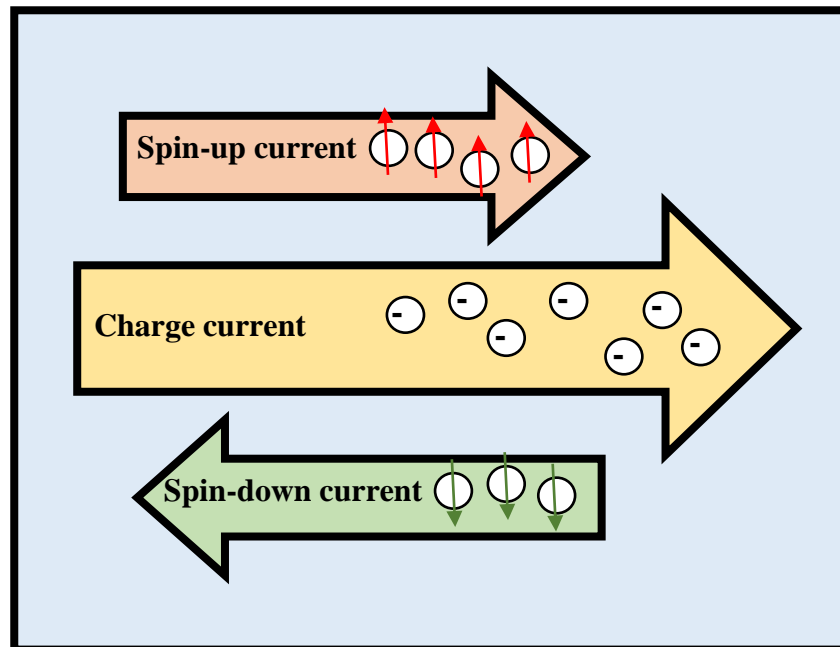

Figure 1-1: Schematic diagram of charge current and spin-dependent current.

Based on similar idea, valleytronics which uses valley degree of freedom was proposed, and more recently pseudospintronics which uses pseudospin degree of freedom was proposed. Valley is the local maximum of valence band or minimum of conduction band in semiconductor. In contrast to spin which exists in the real-space, valley exists in momentum-space, which sometimes is called reciprocal space or K-space. Another degree of freedom that has been exploited recently is pseudospin. Although with the name pseudospin, it has nothing to do with real spin. It is the degree of freedom unique to materials with honeycomb lattice such as graphene and silicene, where there are two sublattices in one unit cell. We will revisit valley degree of freedom and pseudospin of freedom in more details in Chapter 3.

In short term, spintronics, valleytronics, and pseudospintronics are expected to increase the computing speed, which may be economically difficult with the traditional electronics. However, what attracts much attention to semiconductors-based spintronics and its relatives is the long-term ambitious goal to realize quantum computer. Spin, valley, and pseudospin degree of freedom are concepts from quantum mechanics. Therefore spintronic, valleytronic, and pseudospintronic devices are perfect candidates for quantum computing which uses quantum bits or qubits instead of bits in conventional electronics. With qubits and the superposition of them that allows multiple states at the same time, quantum computer is expected to be much faster than classical computers contributing to the advance of technology.

1.2 Two-Dimensional Dirac Materials

In this section, we briefly introduce a new class of materials which is expected to play important role in spintronics and valleytronics. They are called Dirac materials. Dirac materials are classified as a group of materials in which their electrons behave like massless Dirac particles obeying Dirac equation instead of Schrodinger equation like electrons in other materials [13]. It includes wide variety of materials, such as elemental two-dimensional materials, d-wave superconductor, superfluid materials, and topological insulators [14]. Dirac equation is relativistic wave equation, which is the quantum mechanics that takes

theory of special relativity into account. Dirac equation is normally used in particle physics where particles move in high energy close to the speed of light. By giving Fermi velocity as the effective speed of light in the materials, the wave equations of the materials would be in the form that obeys Dirac equation. Here, Fermi velocity is the electron's velocity with which the electron when travel when it has Fermi energy. When the temperature is low, Fermi velocity can be used as an approximation of electrons' velocity in the materials.

Another common characteristic of Dirac materials, despite being hugely different materials, is the existence of Dirac cone and Dirac point in the band structure. Figure 1-2 shows the schematic diagram of Dirac cone and Dirac point. The name of Dirac cone comes from the linear shape of the band structure around Dirac point. The unique shape of Dirac cone gives rise to very high carrier mobility and many novel phenomena, such as fractional quantum Hall effect (FQHE) and Klein tunneling [15].

Some Dirac materials are two-dimensional, while some are three-dimensional materials. Among wide variety of Dirac materials, elemental two-dimensional Dirac materials, such as graphene and silicene attract particularly much attention. The reason is because they have crystalline structure and have high potential for spintronic applications, unlike their exotic counterparts such as *d*-wave superconductor and superfluid materials.
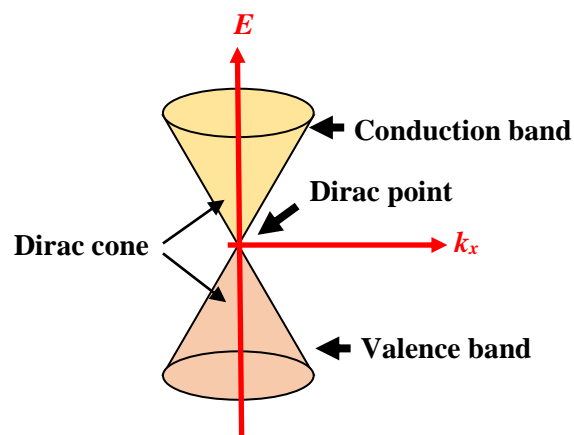

Figure 1-2: Schematic diagram of Dirac cone and Dirac point in Dirac materials.

1.2.1 Elemental Two-Dimensional Dirac Materials

One milestone in spintronics is the isolation of graphene from graphite in 2004. With high electron mobility, long spin lifetime, and long spin diffusion length in room temperature, graphene is a good candidate for spintronics. Since Dirac cone has been observed in graphene, it is considered Dirac material. Moreover, the experimental discovery of graphene opened up a new era for discovery of other elemental two-dimensional (2D) materials.

Currently, the research in two-dimensional materials or single-layer materials has intensified, and many of them have been discovered. There are wide varieties of two-dimensional materials, for instance, elemental materials, compound materials, and organic materials. Dirac cones cannot be observed in most 2D materials, which can be explained with Neumann–Wigner theorem [15], and the intriguing phenomena unique to Dirac materials cannot be expected. Therefore elemental 2D materials, which is a group of single-layer elemental materials, has attracted much attention due to the observation of Dirac cone in graphene. Along with graphene and silicene, there are other materials that possess similar unique characteristics. This group of materials includes graphene (C), silicene (Si), germanene (Ge), stanene (Sn), borophene (B), phosphorene (P), plumbene (Pb), with more materials under investigation [15-20].

One common characteristic of elemental 2D materials is the honeycomb lattice structure. This hexagonal lattice was once considered to be the source of Dirac cone, but it is uncovered recently that the cause of Dirac cone might be mirror symmetries of the materials [21]. However, the honeycomb lattice structure results in existence of two atoms in one unit cell, and gives rise to two sublattices, A and B. These two sublattices contribute to a new concept called pseudospin which will be described in Chapter 3.

1.2.2 From Graphene to Silicene

Among elemental two-dimensional Dirac materials, graphene was the first in the world being discovered in 2004. The discovery has led to Nobel Prize in Physics 2010. It has caused excitement around the world not only in science

community but also in business community, since it was considered to revolutionize many industries, for example, battery, solar cells, pressure sensors, and supercapacitor [22-24]. There are also many proposals to use graphene for spintronic applications, such as spin transistor, spin valve, and spin filter [25-27]. The applications of graphene expand beyond electronics to other area such as mechanical engineering due to the thin and strong properties of single-layer carbon atoms [28]. However, with the discovery of other elemental 2D materials, graphene has become less attractive as a candidate for high-speed electronics and spintronics.

There is no doubt that graphene has contributed to the advance of technologies in many area and possesses properties to be exploited more in the future. However, it is considered that graphene may not an ideal material for spintronic applications due to the absence of bandgap. Although there were successful efforts to open and tune the band gap in graphene [29-31], the processes are not simple comparing to other candidate such as silicene where the band gap can be tuned by electric field. In addition to the existence of band gap which is tunable by electric field, there are other reasons that make silicene shine out among graphene and other elemental 2D materials in the post bulk-silicon era.

One reason is that silicene has longer spin diffusion time and larger spin-orbit coupling than graphene [32]. Spin-orbit coupling is an interaction between the electron's spin with the magnetic field generated by the orbiting electron around the nucleus. It is well known that spin-orbit coupling results in shifts of energy level and causes the splitting of spectral line, a phenomenon known as the Zeeman effect. In relation to spintronics, spin-orbit coupling allows manipulation of electron spin in the absence of magnetic field, and expand the scope of spintronic applications [33]. This makes semiconductor materials with big spin-orbit coupling desirable for spintronics. The presence of large spin-orbit interaction also give rise to the coupling of spin-valley and lead silicene to be a candidate for these growing fields of spin-valleytronics [34]. Another reason is the amount of knowledge and knowhow accumulated in the silicon-dominated semiconductor industry. The successful synthesis of silicene recently also play important role to make silicene a promising candidate for spintronic applications in the future [35].

1.3 Dissertation Overview

In recent years, the number of experimental and theoretical reports on carrier transport in silicene has been increased rapidly. While there have already been few studies in the fundamentals of photo-irradiation effect on silicene, in this dissertation, our original study focuses on the photo-irradiation effect combining with impact of electric field and magnetic exchange field on unexplored dual ferromagnetic-gated silicene junction. We particularly aim at achieving useful applications in spintronics. In the first half of this dissertation, we explain the fundamentals of silicene and elemental two-dimensional Dirac materials in general. We also introduce some parts of quantum mechanics and other theories related to this study. The second half of this dissertation discuss our proposed device structure, as well as the impact of photo-irradiation, electric field, and exchange field on the carrier transport in the device structure.

In Chapter 2, we explain the electronic properties of silicene as well as review the current development in silicene research, since the goal of this study is to understand the electronic transport of silicene and find the potential for device applications in the future. Silicene is a newly found two-dimensional material, where its electrons are governed by quantum mechanics. Therefore, there are many interesting phenomena unusual in three-dimensional materials. The research area in silicene can be categorized into experimental, theoretical, and simulation. Our research presented in this dissertation is theoretical study using tight-binding model. Therefore in Chapter 3, we introduce theory and concepts used in the electronic transport analysis in this study. First, we explain tight-binding model for silicene. It is a powerful and widely used model to analyze electronic transport in condensed matter. Next we introduce the concept of spin, valley, and pseudospin, which are the core concepts being used in our study. Particularly, valley and pseudospin are relatively new concept but have high potential for device applications in the post bulk-silicon era. We also explain magnetic exchange field, another relatively new concept, but very critical for controlling spin and valley in silicene. Cramer's rule which is a useful theorem for solving matrix equation is also explained in this chapter along with the computer environment being used in our analysis.

In Chapter 4, we investigate the carrier transport in our proposed dual ferromagnetic-gated silicene junction. We discover that it is possible to control the device to behave as pure spin polarizer, valley polarizer and pseudospin polarizer by changing the exchange field configuration. After that, we investigate the effects of photo-irradiation in dual ferromagnetic-gated silicene junction in Chapter 5. The results show clear impact of photo-irradiation on spin polarization, valley polarization, and tunnel magnetoresistance. In Chapter 6, we investigate the characteristics of spin-valleytronic photo-sensing silicene device under the photo-irradiation. The study provides an evidence of spin-valley filtering by adjusting electric field and exchange field configuration. Finally, Chapter 7 summarizes this dissertation and briefly discuss the future work.

Chapter 2

Silicene

The isolation of graphene has inspired many scientists to discover other two-dimensional (2D) materials. Among the newly discovered artificial elemental 2D materials, silicene (Si) is considered to be the most promising candidate for the post-bulk-silicon-era electronics, spintronics, valleytronics and quantum computing applications. One reason is the properties of silicene, and another reason is the accumulation of silicon-related technology and knowhow in semiconductor industry [36, 37].

This chapter cover the fundamentals of silicene and the research in silicene before the presentation of our proposed our silicene-based device in Chapter 4. In this chapter, we describe the crystal structure of silicene as well as the overview of basic theory for silicene in Section 2.1. We especially explain the electronics properties of silicene, of which arises from spin-orbit coupling, and could be considered as a topological insulator material in Section 2.2. Finally, we review the silicene research in Section 2.3.

2.1 Introduction of Silicene

Silicene is a Dirac material with honeycomb lattice structure like graphene, but has larger spin-orbit coupling. Therefore, it recently attracted much attention as a promising candidate for spintronic applications. Silicene is two-dimensional silicon with stable out-of-plane bucklings, which arises from mixing between sp^2 and sp^3 hybridization [38]. In graphene, each carbon atom has σ bonds with the adjacent three carbon atoms via sp^2 hybridization, and each hexagonal ring has one π bond orienting out of plane. The stability of the planar structure in graphene

occurs because of the short distance between adjacent carbon atoms, while π orbitals are responsible for the many exciting electronic properties.

On the other hand, silicon atoms have larger atomic radii and prefer sp^3 hybridization as found in the diamond structure of bulk silicon, rather than sp^2 hybridization. Therefore, it has mixing of sp^2 and sp^3 hybridization in the planar structure with buckling for stability [39, 40]. Figure 2-1 shows the image of lattice structure of silicene with both three-dimensional view and side view. It indicates that sublattice-A and sublattice-B are displaced in the out-of-plane direction, and each of them locates on different plane. Figure 2-2 depicts the unit cell of silicene lattice, where there are two atoms in one unit cell resulting in two sublattices, A and B.
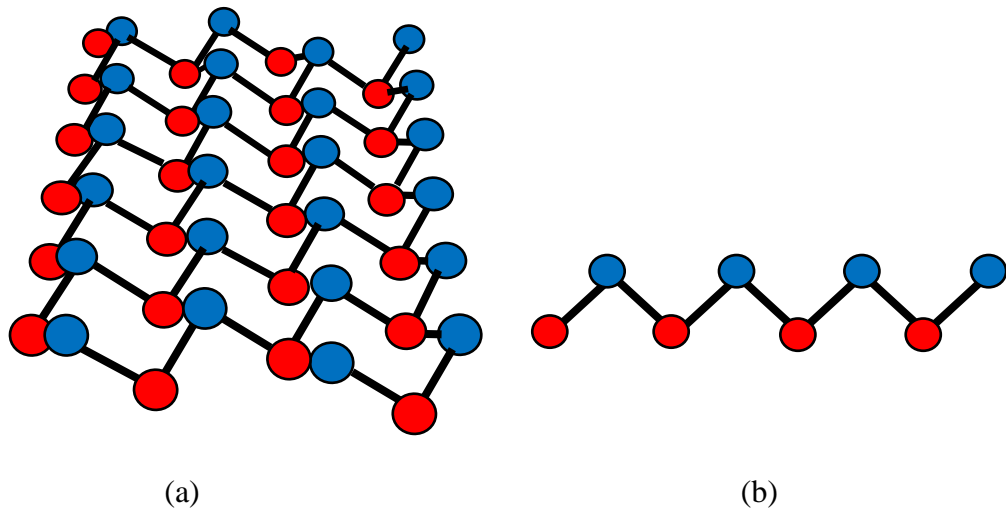

(a) (b)

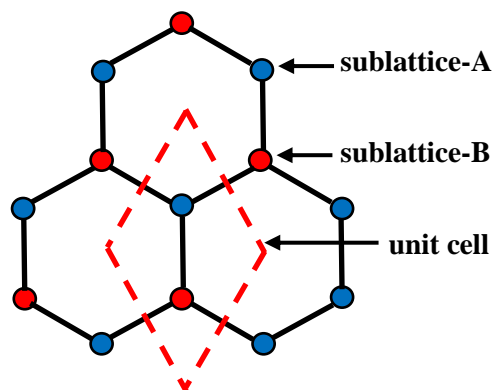Figure 2-1: Lattice structure of silicene (a) Three-dimensional view. (b) Side view.

Figure 2-2: Top view of the unit cell of silicene lattice with two sublattices.

Honeycomb lattice has two sublattices in one unit cell, because it is not a Bravais lattice and two neighboring sites in the lattice are not equivalent. Bravais lattice is a lattice structure that looks exactly the same from any lattice point. The position vector r of a lattice point can be described by primitive translational vectors as

$$r = n_1 a_1 + n_2 a_2 + n_3 a_3, \tag{2.1}$$

where n_1, n_2, and n_3 are any integers. When a is nearest-neighbor distance, the primitive translational vector a_1, a_2, a_3, can be described as

$$a_1 = \frac{1}{2} a(\vec{x} + \vec{y} - \vec{z}) \, , \, a_2 = \frac{1}{2} a(-\vec{x} + \vec{y} + \vec{z}) \, , \, a_3 = \frac{1}{2} a(\vec{x} - \vec{y} + \vec{z}) \, . \tag{2.2}$$

However, the lattice points at sublattice-A and sublattice-B are not exactly the same as illustrated in Figure 2-3. The sublattice-A in one unit cell has its nearest-neighbor atoms in northwest, northeast, and south, while the sublattice-B has its nearest-neighbor atoms in north, southwest, and southeast. Therefore, honeycomb lattice can be viewed as a triangular or hexagonal Bravais lattice with a two-atom basis, where basis is one or group of atoms repeated at each lattice point. The three vectors that connect an atom at sublattice-A with its nearest-neighbor atoms can be described as

$$\mathbf{A_1} = \frac{1}{2} a(\sqrt{3}\vec{x} + \vec{y}) \, , \, \mathbf{A_2} = \frac{1}{2} a(-\sqrt{3}\vec{x} + \vec{y}) \, , \, \mathbf{A_3} = -a(\vec{y}) \, . \tag{2.3}$$
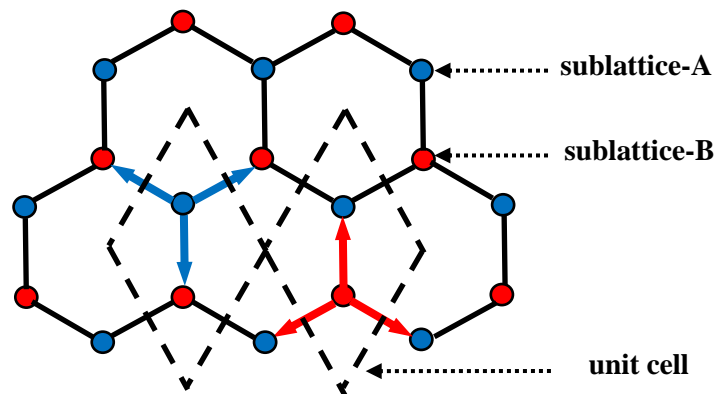

Figure 2-3: Difference between sublattice-A (in blue) and sublattice-B (in red).

One obstacle to the applications of silicene is the availability of free-standing silicene. Currently, it is considered impossible for free-standing silicene to exist due to the strong electron correlation in silicon-based nanostructures [41]. However, there are many studies reported successful synthesis of monolayer silicene and multilayer silicene on many kinds of substrates, which will be introduced in more details in Section 2.3. It was also found that the characteristics of silicene layer are sensitive to the substrate. This surface sensitivity of silicene is due to mixed sp^2 and sp^3 hybridization [42]. The buckling height of the silicene layer is also sensitive to substrates. The result from first-principle calculations shows that the honeycomb structure of free-standing silicene would be stable with low-buckled structure with buckling height at 0.44 Å [43]. It was also reported that the buckling height of the silicene layer might be affected by the substrates that it is synthesized on [44]. Therefore, substrates play important role on the properties of synthesized silicene layer, since the buckling height is a crucial factor for the electronic transport in silicene.

2.2 Electronics Properties of Silicene

Silicene has atomic structure akin to graphene, but with out-of-plane buckling. Therefore, some properties of silicene are different from those in graphene, a relatively well understood predecessor. Two main characteristics differing silicene from graphene are the large spin-orbit coupling and the buckled structure. In this section, we will explain the electronics properties of silicene, which is critical for electronic and spintronic applications, in relation to the spin-orbit coupling and buckle structure. Topological insulator is also another crucial concept for silicene [45], and we would like to introduce here.

Topological insulators (TI) are a group of exotic matters with a lot of interesting properties. They are materials that can be characterized by an insulating band gap inside the bulk of the materials, and gapless band structure on the edge or surface. This makes topological insulators behave as insulators internally, but behave as conductors on the surface. This state of matter could be realized with the combination of spin-orbit interactions and time-reversal symmetry [46]. Topological insulators are highly expected as materials to realize quantum

computation based on spintronics. The concept of topological insulators have emerged from the discovery that spin-orbit coupling can lead to topological insulating electronic phases [47]. It is another class of materials that has been investigated actively recently for the spintronic applications and quantum computation due to their special properties on the surface states. The state of two-dimensional topological insulator is quantum spin Hall state which is a phenomenon related to family of Hall effects [48].

Quantum spin Hall effect (QSHE) is closely related to quantum Hall effect (QHE) [49, 50]. Quantum Hall effect is a quantum-mechanical version of the Hall effect, where Hall conductance is quantized. It occurs in two-dimensional materials under strong magnetic field resulting in one-dimensional current channel on the edge flowing in one direction as illustrated in Figure 2-4(a). There is no spin-dependent current in QHE. On the other hand, quantum spin Hall effect, which is a state representing topological insulator, is similar to quantum Hall effect. However, magnetic field is not required. Moreover, the spin-dependent currents flow in opposite direction due to spin-orbit coupling. Realization of quantum spin Hall effect requires a coupling between the spin and the orbital motion of electrons. The main mechanism of this requirement is band inversion, in which the conduction band and valence band is inverted by spin-orbit coupling [51]. Hence, not all materials that possess spin-orbit coupling could be topological insulator and show quantum spin Hall effect, since the inversion of conduction band and valence band cannot occur in all materials. Figure 2-4(b) shows the schematic diagram of QSHE, where the spin-up current flows in counterclockwise direction and the spin-down current flows in clockwise direction.

Quantum spin Hall effect is quite different from another phenomenon related to Hall effect, which is called spin Hall effect (SHE). Spin Hall effect is the phenomenon that has already been applied widely in spintronics [52, 53]. Spin Hall effect can be described as a phenomenon that the electron's spin with opposite sign would accumulate on the opposite side of the conductor as the result of spin-orbit coupling. This is because spin-orbit coupling causes interaction between the spin and the charge of electrons. As the result, the charge current may induce accumulation of electron spins and gives rise to spin current in the absence of magnetic field.
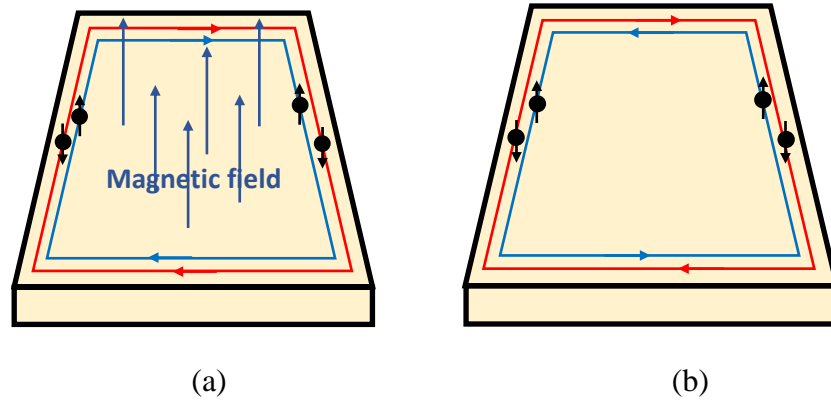
Figure 2-4 Schematic diagram of (a) quantum Hall effect (QHE), (b) quantum spin Hall effect (QSHE).

Silicene along with other novel 2D materials, especially stanene and plumbene, have relatively large band gap opening and spin-orbital coupling strong enough to maintain robust quantum spin Hall states at high temperature, which makes them topological insulators. Interestingly, silicene can become both a semiconductor and a topological insulator with appropriate control of external electric field [54]. The spin-orbit coupling also provides an energy gap to the Dirac point. The abovementioned desirable characteristics are difficult to achieve in graphene due to the small ionic radius of carbon. The large spin-orbit coupling is the result of large ionic radius and the buckled structure, which makes silicene to behave as a two-dimensional topological insulator [55]. The strong spin-orbital coupling also gives rise to the spin-valley coupling, which may lead to the integration of spintronics and valleytronics [56, 57]. The concept of valley, the local maximum of valence band or minimum of conduction band in semiconductor, would be explained in more details in Chapter 3.

In addition to stronger spin-orbit coupling, another main characteristic of silicene that is different from graphene is the out-of-plane buckling. Buckled structure allows the band gap of silicene to be manipulated by electric field [58, 59]. It also causes tunable spin-valley coupled band structure giving rise to topological phase transition, an intriguing transport phenomenon [60]. Topological phase transition is the transition from one topological phase to another phase, for example, from topological insulator to band insulator. Silicene is rich in term of topological phases such as quantum spin Hall state, quantum anomalous Hall state,

quantum Hall effect state, fractional quantum Hall effect state, and band insulator. When the electric field and exchange field are controlled appropriately, it is possible to realize these phases and achieve the topological phase transition [54, 58]. Exchange field could be approximately considered as a magnetic field. The more detailed explanation of exchange field would be provided in Chapter 3.

2.3 Trends in Silicene Research

Silicene has many interesting properties with the great potential for applications in spintronics and quantum computation. Hence, it is one of the most active research area with fierce competition in recent years. One of the unique trends in silicene research is the extensive use of computational modelling method, in addition to theoretical and experimental research. The reason is the computational cost that has decreased dramatically, and the increasing accuracy of density functional theory (DFT). In this section, we review the progress on silicene research in general, and focus particularly on the area that is related to our study in electronic transport, spin-valley polarization, and photo irradiation effect.

Silicene has relatively stronger spin-orbit coupling than graphene which gives rise to the spin-valley coupling [61]. There have been many theoretical and computational studies in spin-valley transport in silicene junctions, which helps the progress in this area. The topics of study are, for instance, the mechanism of magnetism that opens different spin-dependent band gaps at k and k' points and results in spin and valley polarized transports [61], the conditions of electric field for the fully valley and spin polarized transports [62], ballistic transport through silicene ferromagnetic junctions under the presence of magnetic exchange field and normal electric field [63], as well as the transmission probability and valley conductance in relation to the electric field and magnetic exchange field [64]. There is also study on spin thermoelectric properties of zigzag silicene nanoribbons doped with cobalt atoms [65].

Another research area that has been very active is electronic transport of spintronic and valleytronic devices based on silicene, such as spin filter and spin-valley filter [66-68], spin-polarized transport in a dual-gated silicene system where there is no exchange field [69], and using electric field and exchange field to tune

the plasmonic response of the electron gas [70], where plasmon is a quantum of electron density oscillation. In addition to spin current and valley current, there is pseudospin current in silicene, which is the current that flows in either A or B sublattice-Atomic structure. It was suggested that the pseudospin currents could be used for pseudospintronics. Recently, double ferromagnetic-gated silicene junction was proposed to control pseudospin current along with pure spin-valley current in silicene giving a possibility for pseudospintronics [71]. The recent study on field-effect transistors operating at room temperature made from silicene [37] is particularly considered to be a great achievement in devices development area.

The effects of photo irradiation on silicene have also been investigated. It was discovered that photo irradiation has effects on the band structure of silicene, where circularly polarized light is used to open a gap at the Dirac point [72]. By irradiation of circularly polarized light under electric field, the topological class of silicene could be changed from quantum spin Hall insulator to other phase [73]. Another study found that the photo-irradiation helps realizing a topological superconductor when s-wave superconductivity proximity coupling is applied to silicene [74]. It is also reported that spin polarization and valley polarization in silicene are related to the intensity of the irradiated off-resonant circularly polarized light as well as electric field, and the polarization can be inverted by reversing the direction of electric field or the circular polarization of the light [75]. It was also discovered that spin-valley polarizations and tunneling magnetoresistance in a ferromagnetic-normal-ferromagnetic junction can be significantly enhanced by off-resonant circularly polarized light without the presence of electric field or magnetic field [76]. There is also a study in effective photo-induced band structure manipulation with intense terahertz irradiation beyond the off-resonant condition [77].

In other research area, there is interesting development in hydrogenation, a chemical reaction to add hydrogen atoms to the material. The fully hydrogenated silicene is called silicane. It was investigated through density functional theory that the energy band gap of silicene might be altered by hydrogenation, and give silicane a potential in optical applications [78]. Furthermore, it was suggested that silicane could be used as substrate for silicene to make high-speed field effect

transistor [79]. On the other hand, half-hydrogenated silicene was suggested to be a method to introduce magnetism and generate band gap in silicene [80].

In the area of synthesis, experimental groups have succeeded in synthesis of multilayer silicene using both epitaxial growth and non-epitaxial growth after theoretically proposal, in addition to synthesis of monolayer silicene on Ag, ZrB_2, and Ir substrates, [81-83]. Besides the synthesis, there is another interesting research area on the modification of silicene sheet through strain. There is one study on the self-doping phenomenon induced by strain in silicene sheet using first-principle calculations. It was reported that the silicene nanosheet behaves as n-type doped silicene under compressive strain, while behaves as p-type doped silicene under tensile strain [84].

Although many studies have been done on various aspects of silicene, more analysis and investigation must be done to have better understanding in the properties of this 2D material for being used in real-world applications.

Chapter 3

Theory and Methodology

The research in silicene has been done actively in recent years, and we have reviewed parts of them in Chapter 2. Silicene research can be categorized into experimental, theoretical, and computational studies. Our investigation is in the category of a theoretical study using tight-binding model, and then Mathematica is used to help solving the equation. It is easy to become confused between the theoretical and computational study, especially when a computer program such as Mathematica is used to assist the calculation. Hence, we give the overview of methodology in theoretical study and compare it to that in computational study in Section 3.1. We also introduce Mathematica and the overview of computer algebra system in this section. Section 3.2 explains the tight-binding model and the Hamiltonian obtained from the model, which is the core of theoretical study. We introduce the basic theory of spin, valley, and pseudospin, which are important concepts being used in our investigation, in Section 3.3. In Section 3.4, magnetic exchange field which is another crucial concept being used throughout this study is explained. Section 3.5 give the overview of the Cramer's rule, an important mathematical theorem we use to solve the matrix equation before running Mathematica to find the numerical values of the coefficients.

3.1 Introduction

In this section, we give the overview of theoretical methodology being used to analyze electronic transport in silicene. We particularly differentiate the theoretical study from computational study, since it is easy for them to cause confusion. In general, theoretical study uses mathematical model and abstractions

to explain and predict the phenomena, while experimental study uses tools and equipment to synthesize, fabricate, and measure the physical objects. In our study, tight-binding model and quantum mechanics are used extensively as the tool in theoretical analysis. With the prevalent of affordable computing power and good symbolic computation software such as Mathematica, we can use computer programs as a tool to help solving the problem theoretically.

Symbolic computation is different from numerical computation which is more familiar in engineering. The key in symbolic computation is the computer algebra system which is a type of software that uses mathematical expression containing variables without knowing the values, and does the computation by using those variables as symbols [85]. In symbolic computation, great efforts are put on the exact computation by using smart mathematical algorithm and simplifier for mathematic formula. Some examples of computer algebra system are Mathematica, Maple, and Mathcad. On the other hand, numerical computation or numerical analysis uses numerical approximation approach to solve problems while accepting reasonable errors [86]. Examples of widely used numerical analysis software are Matlab and GNU Octave.

The easy access to computing power also gives rise to another methodology called computational study, or computer simulation. It uses mathematical model to imitate the behavior of the system in computer [87]. Computer simulation has been very helpful for experimental studies when the cost of the experiment is high, for example, in semiconductor device fabrication and aerospace development. In recent years, computer simulation has also been used extensively in other fields of study, such as physics, material science, chemistry, biology, economics, and social science. There are many methods being used for computer simulation. In the field of physics and material science, density functional theory (DFT) is a very successful method that uses quantum mechanics to solve problems in quantum many-body systems with large number of interacting particles [88]. It calculates the electronic structures, particularly the ground states of the materials. Although density functional theory cannot provide absolute accuracy since it uses many approximations, it could provide good prediction for properties of the materials. The results from density functional

theory were considered inaccurate in the past, but the situation has been improved with the refinement of approximations being used.

Other successful simulation methods include semiempirical method and Monte Carlo method [89]. Both theoretical study and computational study may use computation, but the tools they use and the expected output from them are different. In theoretical study, tight-binding model is a widely used tool to analyze the electronic structures of the materials. Other popular quantum mechanical tools in theoretical study include nearly-free electron model, where electrons can move almost freely through the lattices. We introduce the tight-binding model in the next section.

3.2 Tight-Binding Hamiltonian

Tight-binding model is a widely used fully-quantum-mechanical-approach to analyze the electronic band structure of the materials. It is an approximation to obtain the Hamiltonian, which is the total energy of the system and is necessary to analyze a system. Tight-binding model uses one electron approximation, where each electron is tightly-bound to the belonged nuclei. One electron approximation does not take account of the interaction with other electrons and external potentials, but instead it uses superposition of wave functions of isolated atoms to obtain the total wave function of the system [90, 91].

In a system with N atoms, the time-independent Schrodinger equation of a single electron can be expressed as

$$H\Psi(\vec{r}) = E\Psi(\vec{r}) , \qquad (3.1)$$

where H is Hamiltonian, E is the excited energy, $\Psi(\vec{r})$ is the atomic wave function, and r is the interatomic distance. To solve the eigenvalue problem in Equation 3.1, the Hamiltonian matrix elements between atomic orbitals at different interatomic distances are required. In general, Hamiltonian can be described by

$$H = -\frac{1}{2}\nabla^2 + V(\vec{r}) , \qquad (3.2)$$

where $V(\vec{r})$ is the potential energy. A typical approximation in tight-binding model is to assume that electrons can hop only to the nearest-neighbor atom, but we might also need the next-nearest-neighbor hopping terms to describe the system in some cases. The transfer integral which determine the rate of electrons moving from one site to another is called hopping integral in tight-binding model, and it is related to the distance between atoms.

In silicene, the tight-binding Hamiltonian can be well described with

$$H = -t \sum_{\langle i,j \rangle \alpha} c_{i\alpha}^{+} c_{j\alpha} + i \frac{\Delta_{SO}}{3\sqrt{3}} \sum_{\langle\langle i,j \rangle\rangle \alpha\beta} v_{ij} c_{i\alpha}^{+} \sigma_{\alpha\beta}^{z} c_{j\beta} - i \frac{2}{3} \Delta_{R2} \sum_{\langle\langle i,j \rangle\rangle \alpha\beta} t_{z}^{i} c_{i\alpha}^{+} (\sigma \times \hat{d}_{ij})_{\alpha\beta}^{z} c_{j\beta} , \quad (3.3)$$

where the creation operator $c_{i\alpha}^{+}$ creates an electron with spin polarization α at the atomic site i of the lattice structure, $\langle i, j \rangle$ ranges for all over the nearest-neighbor atoms, and $\langle\langle i, j \rangle\rangle$ ranges for all over the next-nearest-neighbor atoms [34]. The first term of Equation 3.3 indicates the nearest-neighbor hopping with the hopping energy $t = 1.6$ eV, while the second term represents the effective spin-orbit coupling with $\Delta_{SO} = 3.9$ meV. The next-nearest-neighbor hopping parameter is $v_{ij} = +1$ when the hopping direction is counterclockwise, and $v_{ij} = -1$ when the hopping direction is clockwise in relation to the z axis. The third term represents Rashba spin-orbit interaction $\Delta_{R2} = 0.7$ meV, where $t_{z}^{i} = +1$ for sublattice-A and $t_{z}^{i} = -1$ for sublattice-B at the atomic site i. The notation $\hat{d}_{ij} = d_{ij} / |d_{ij}|$ represents the connection between two atomic sites i and j in the same sublattice.

At the low energy near Dirac point, at which electrons obey the Dirac equation resulting in many exotic phenomena, the effective Hamiltonian can be described with Dirac theory as

$$H^{0} = \hbar v_{F} (\eta k_{x} \tau_{x} + k_{y} \tau_{y}) + \Delta_{SO} \eta \tau_{z} \sigma_{z} + a \Delta_{R2} \eta \tau_{z} (k_{y} \sigma_{x} - k_{x} \sigma_{y}), \quad (3.4)$$

where v_{F} is the Fermi velocity, silicene lattice constance $a = 3.86$ Å, $\vec{\tau} = \langle \tau_{x}, \tau_{y}, \tau_{z} \rangle$ is Pauli spin-operator for sublattice pseudospin, $\vec{\sigma} = \langle \sigma_{x}, \sigma_{y}, \sigma_{z} \rangle$ is

Pauli spin-operator for real spin, $\eta = 1$ denotes valley k, and $\eta = -1$ denotes valley k', and $\vec{k} = \langle k_x, k_y, k_z \rangle$ is wavevector [34].

There are four main external potentials that can be used to control the band gap: electric field, photo irradiation, magnetic exchange field, and chemical potential. Taking into account all of the potentials, then the Dirac Hamiltonian can be described with

$$H = H^0 - lE_z\tau_z + \eta\lambda_\Omega\tau_z + \Delta M\sigma_z\tau_z + \mu + \overline{M}\sigma_z, \tag{3.5}$$

where l is the distance between sublattice, E_z is the external electric field, λ_Ω represents the applied photo irradiation, $\Delta M = M_A - M_B$ is the applied magnetic exchange field where M_A is the exchange field on sublattice-A and M_B is the exchange field on sublattice-B, respectively. $\overline{M}$ is the mean of applied magnetic exchange field, and μ is chemical potential [34]. We use effective Hamiltonian based on Equation 3.5 in our investigation.

We can calculate the band structure of silicene by using tight-binding model. Since the real crystal is three-dimensional, the real band structure that we consider should be three-dimensional, too. However, it is more common to look at the two-dimensional band structure of the lattice structure to grasp information, because it is easier to produce and the information is sufficient in most cases. Figure 3-1 shows the two-dimensional band structure diagram of silicene obtained from tight-binding model [92]. Dashed lines show the result from tight-binding method, while the solid lines are the results from ab initio calculations. The band structure exhibits linear dispersion or Dirac cone at point K in the reciprocal space. The Fermi velocity v_F is estimated to be around 10^6 m/s [43] which is comparable to the value obtained from first-principles calculation, and is similar to graphene. However, the band gap estimated from tight-binding model is 7.9 meV, which is different from the more accurate value of 1.55 meV obtained from density functional theory [55].
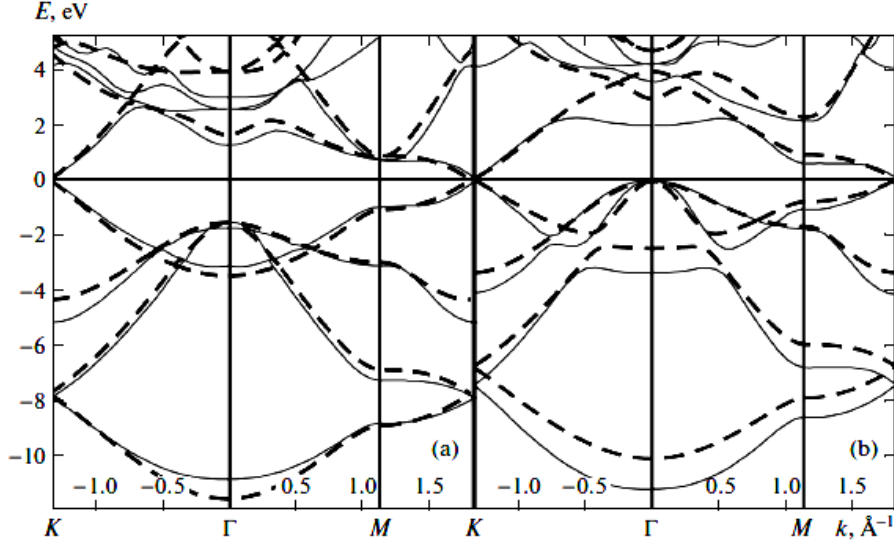
Figure 3-1: Band structure of silicene from tight-binding model [92].

3.3 Spin, Valley and Pseudospin

Spin is one of intrinsic degree of freedom of electrons along with charge, and is a pure quantum mechanical concept. Using spin degree of freedom allows us to expand the technology beyond electronics into spintronics. In this section, we explain the concept of spin degree of freedom, as well as the valley and pseudospin degree of freedom which attract attention recently.

Although elementary particles and atomic nuclei also have spins, we focus on electron's spin in this section. Electron's spin is an intrinsic angular momentum of electrons, which is unrelated to the spinning motion misled by the terminology 'spin'. Electrons have half-integer (1/2) spin making it to be categorized as fermions. The quantum state of electron's spin can be described by a spinor, a two-component complex-valued vector. The observable of the spin can be expressed with spin operators (S_x, S_y, S_z), which can be described by 2×2 complex matrices called Pauli matrices. In quantum mechanics, states are described as vectors in a vector space, and the observables which are the things that we measure are described by operators [93]. The three spin operators are

$$S_x = \frac{\hbar}{2}\sigma_x = \frac{\hbar}{2}\begin{bmatrix} 0 & 1 \\ 1 & 0 \end{bmatrix}$$

$$S_y = \frac{\hbar}{2}\sigma_y = \frac{\hbar}{2}\begin{bmatrix} 0 & -i \\ i & 0 \end{bmatrix}$$

$$S_z = \frac{\hbar}{2}\sigma_z = \frac{\hbar}{2}\begin{bmatrix} 1 & 0 \\ 0 & -1 \end{bmatrix}, \tag{3.6}$$

where the operator S_x, S_y, and S_z affects a measurement of the spin in the x, y, and z direction, respectively. The notations σ_x, σ_y, and σ_z are Pauli matrices, and can be summarized as

$$\sigma_x = \begin{bmatrix} 0 & 1 \\ 1 & 0 \end{bmatrix}, \ \sigma_y = \begin{bmatrix} 0 & -i \\ i & 0 \end{bmatrix}, \ \sigma_z = \begin{bmatrix} 1 & 0 \\ 0 & -1 \end{bmatrix}. \tag{3.7}$$

There are two eigenvalues of the operator S_z: $+1/2$ and $-1/2$, where the spin up and spin down are described respectively by eigenspinors as

$$\left| s_z = +\frac{1}{2} \right\rangle = |\uparrow\rangle = |0\rangle, \ \left| s_z = -\frac{1}{2} \right\rangle = |\downarrow\rangle = |1\rangle. \tag{3.8}$$

Another degree of freedom that has attracted attention recently due to its potential for applications in quantum computation is valley degree of freedom. The valley degree of freedom is based on two sets of inequivalent and degenerate Dirac points at k and k'. Valley degree of freedom could lead to valleytronics which is expected as a pathway towards quantum computation. Valley is the local maximum of valence band or minimum of conduction band in semiconductor, which exists in reciprocal space.

Interestingly, the reciprocal lattice of honeycomb lattice is also a honeycomb lattice. Figure 3-2 shows the band structure of graphene at low energy to describe the concept of valley. The hexagonal shape indicates the first Brillouin zone. The notations k and k' indicate two sets of inequivalent valleys, which arises from the opposite sign of Berry curvature [94, 95]. The Berry curvature $\Omega(k)$ can be described as

$$\Omega(k) = \nabla_k \times \langle u(k) | i\nabla_k | u(k) \rangle \ , \tag{3.9}$$

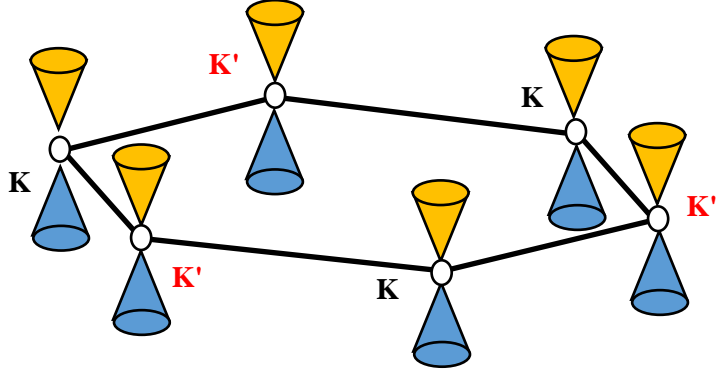where $|u(k)\rangle$ is the periodic part of the Bloch function.

25

Figure 3-2: Band structure of graphene at low energy to show the concept of valley.

The concept of Berry curvature is closely related to Berry phase or geometric phase [96, 97]. Berry phase is a phase difference occurred in a system with cyclic adiabatic process, which is a gradually changing process that the probability density so that can be modified. The terminology of 'geometric phase' comes from the fact that the phase difference is the difference of tangent along the path taken by a particle along the curvature.

More recently, pseudospin degree of freedom in graphene and silicene has been investigated. It is sometimes called lattice pseudospin or sublattice pseudospin to avoid confusion with Anderson's pseudospin in superconductor model. The terminology of pseudospin comes from the fact that an electron in honeycomb lattice has a probability to be in either sublattice-A or sublattice-B, and it can be described mathematically with Pauli matrices like spin. Therefore, the pseudospin in two-dimensional materials indicates sublattices rather than the real spin of electrons [98]. The two pseudospin states Ψ_A and Ψ_B can be expressed as the wave-state components of the electron wave function Ψ in 2D honeycomb lattice structure as follows:

$$\Psi = \begin{pmatrix} \Psi_A \\ \Psi_B \end{pmatrix}. \tag{3.10}$$

Using the Pauli spin matrices, the pseudospin operator $\vec{S}$ can be defined as

$$\vec{S} = \frac{\hbar}{2}(\tau^x a_x + \tau^y a_y + \tau^z a_z),$$
(3.11)

where τ^x, τ^y, and τ^z are Pauli spin matrices, and a_x, a_y, a_z are unit vectors in x, y, and z direction, respectively. Although the terminology is similar, spin and pseudospin are quite different. Spin is a quantized intrinsic angular momentum of an electron, while pseudospin can be considered as a sublattice index of an electron. Therefore, pseudospin polarized current may be considered as sublattice-dependent current.

3.4 Magnetic Exchange Field

There have been reports on the effects of magnetic exchange field, or exchange field, in silicene [63, 99]. In this section, we explain the concept of magnetic exchange field. When electronic wavefunctions of neighboring electrons overlap, the electrons' spin displays quantum mechanical interaction, which causes energy splitting between spin-up electrons and spin-down electrons. The spin interaction is called exchange interaction or exchange coupling, and the energy splitting is called exchange splitting or exchange energy. When the exchange interaction occurs between a magnetic atom and the neighboring atoms, it causes the whole material to become a magnetic material.

One method to produce magnetic exchange field in elemental 2D materials is by using proximity effects, where the deposition of ferromagnetic insulators on graphene induces exchange splitting Δ of about 5 meV [100]. The investigation also shows that the exchange splitting Δ caused by external magnetic field B can be approximately calculated as $\Delta / B \approx 5.8 \times 10^{-2}$ meV/T. Therefore, there is no difference between exchange field and external magnetic field in macroscopic view; however, the mechanism and interactions are different in microscopic view.

In addition to the theoretical proposal, magnetic exchange field has been realized experimentally by deposition of ferromagnetic insulator EuO onto graphene [101]. They reported a successful growth of high-quality crystalline EuO on single-layer graphene with reactive molecular beam epitaxy. This experimental success paves a way towards spintronic and valleytronic devices.

3.5 Cramer's Rule

Cramer's rule is an important mathematical theorem being use to solve the linear equations for one variable without the necessity to handle the whole linear system [102]. In our study, the matrix equations from wave equations need to be solved to calculate the transmission coefficient, which would be used to obtain the conductance of the device. Therefore, we introduce Cramer's rule in this section.

When we have a linear system of equations as follows:

$$x - 2y + 3z = 7$$
$$2x + y + z = 4$$
$$-3x + 2y - 2z = -10.$$

Then we can use matrices to represent the abovementioned equations as

$$\begin{bmatrix} 1 & -2 & 3 \\ 2 & 1 & 1 \\ -3 & 2 & -2 \end{bmatrix} \begin{bmatrix} x \\ y \\ z \end{bmatrix} = \begin{bmatrix} 7 \\ 4 \\ -10 \end{bmatrix}.$$

Then we find the determinant D of the coefficient matrix $\begin{bmatrix} 1 & -2 & 3 \\ 2 & 1 & 1 \\ -3 & 2 & -2 \end{bmatrix}$. In this case, the determinant $D = 15$. Next, we substitute the first column of coefficient matrix with answer column, and calculate the determinant D_x of the matrix. Then we repeat the process with the second and third column to obtain determinant D_y and D_z, of which can be expressed as

$$D_x = \begin{vmatrix} 7 & -2 & 3 \\ 4 & 1 & 1 \\ -10 & 2 & -2 \end{vmatrix} = 30$$

$$D_y = \begin{vmatrix} 1 & 7 & 3 \\ 2 & 4 & 1 \\ -3 & -10 & -2 \end{vmatrix} = -15$$

$$D_z = \begin{vmatrix} 1 & -2 & 7 \\ 2 & 1 & 4 \\ -3 & 2 & -10 \end{vmatrix} = 15.$$

Then the answer can be obtained with

$$x = D_x / D = 30/15 = 2, \quad y = D_y / D = -15/15 = -1, \quad z = D_z / D = 15/15 = 1.$$

Chapter 4

Carrier Transport in Dual Ferromagnetic-Gated Silicene Junction

From Chapter 1 to Chapter 3, we have explained the necessity of transition from electronics to spintronics, and provided the overview of newly found group of materials called elemental 2D materials which attracted great attention due to many exotic properties. We have focused on silicene in particular, and explained its properties. We have also described the relatively unfamiliar concepts that are relevant to our research, such as spin, valley, pseudospin, and magnetic exchange field. In this chapter, we proposed a dual ferromagnetic-gated silicene junction and investigate the electronic transport in this junction.

4.1 Introduction

One of the major milestones in silicene research is to control the spin-polarized current for spintronic applications. In the past few years, researchers have discovered that the spin current can be controlled by external electric field and magnetic exchange field. There are few studies on the control of spin and valley transport by electric field and exchange field in ferromagnetic junctions [62, 63]. One study reported oscillation of spin and valley currents with the length of the ferromagnetic barrier, and found fully polarized spin and valley currents when electric field of 10 meV is applied at the ferromagnetic barrier. The other study has investigated charge and spin transport in single and double ferromagnetic junctions when electric field is applied to the ferromagnetic barriers in a certain configuration of exchange field. The study has focused on the single ferromagnetic

junction, and predicted that the charge conductance as a function of barrier width may change from oscillatory to a monotonical when electric field goes beyond a critical value. They also predicted nearly perfect spin polarization when electric field and exchange field are above certain levels. In addition, they briefly showed the correlation between charge and spin currents with exchange field in double ferromagnetic junctions.

In our study presented in this chapter, we focus on the double ferromagnetic barrier structure, and systematically study the effects of electric field and exchange field on spin polarized current, valley polarized current, and pseudospin polarized current. We also introduce the idea of changing the configuration of exchange field to see the impact on electronic transport in the device structure.

4.2 Device Models

4.2.1 The Basic Device Structure

The proposed structure has two ferromagnetic barriers on top of silicene layer, with metallic gates above the barriers. The ferromagnetic barriers, FM1 and FM2, are L apart from each other with length d for each barrier. The silicene under the barriers are induced into ferromagnetism by a pair of ferromagnetic insulators EuO on both sides of the silicene sheet. The ferromagnetic insulators also generate exchange splitting by proximity coupling [100, 101]. Since silicene sheet has the buckling structure, it has a perpendicular distance between sublattice-A and sublattice-B of 0.46 Å [103]. Therefore different exchange fields can be separately induced into sublattice-A at the top and sublattice-B at the bottom. They are designated as h_{1A} and h_{1B} at FM1, while at FM2 they are designated as h_{2A} and h_{2B}, respectively.

In this proposed structure, external electric fields are applied perpendicularly at the ferromagnetic regions. The chemical potential μ is induced by the top and the bottom gates with the same tunable potential μ/e, where it is the change of energy when electrons are added or removed from the system. Chemical potential is known as Fermi energy at the temperature of zero Kelvin, and the total

chemical potential in semiconductor is known as Fermi level. The chemical potential can be provided by doping the silicene, but we use external potential to adjust the value in our proposed structure. Figure 4-1 shows the schematic model of proposed structure NM1/FM1/NM2/FM2/NM3, where NMs stand for normal regions and FMs stand for ferromagnetic regions.

Tight-binding Hamiltonians has been described in Chapter 3 by Kane-Mele model based on the behavior of non-interacting electrons in NM1, NM2 and NM3 layers [47]. Then the low-energy effective Hamiltonians is used to analyze electronic transport in sublattice-A and sublattice-B under the influence of the electric field, chemical potential, and exchange energy [66]. In this analysis, we consider that the effect of Rashba interaction is very small comparing with the other terms at low energy [34, 62]. Therefore, the wave equation with excited energy E can be described

$$H_{\eta\sigma}\Psi_{\eta\sigma} = E\Psi_{\eta\sigma}, \qquad (4.1)$$

where $\eta = 1(-1)$ represents valley index $k(k')$ and $\sigma = 1(-1)$ represents spin $\uparrow(\downarrow)$, respectively [34, 62, 66]. $\Psi_{\eta\sigma} = \begin{pmatrix} \Psi_{A,\eta\sigma} \\ \Psi_{B,\eta\sigma} \end{pmatrix}$ is the spin-valley dependent lattice-pseudospinnor field, where $\Psi_{A,\eta\sigma}$ is the electronic wave functions at sublattice-A and $\Psi_{B,\eta\sigma}$ is the electronic wave functions at sublattice-B, respectively.
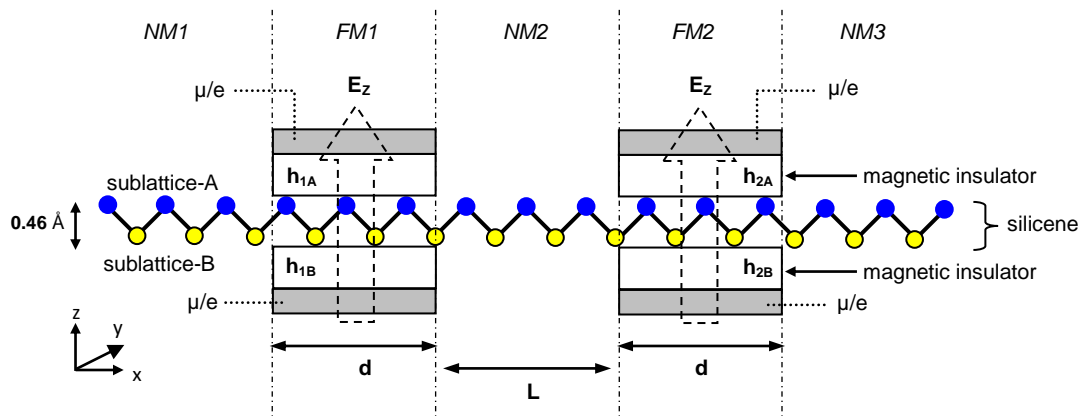

Figure 4-1: Schematic model of proposed structure NM1/FM1/NM2/FM2/NM3.

In the normal regions (NMs) where there is no either electric field or exchange field, the low-energy effective Hamiltonian can be described as

$$H_{\eta\sigma} = v_F(p_x\tau_x - \eta p_y\tau_y) - \Delta_{\eta\sigma}\tau_z, \tag{4.2}$$

where $\hat{p}_x = -i\hbar\dfrac{\partial}{\partial x}$, $\hat{p}_y = -i\hbar\dfrac{\partial}{\partial y}$. The notations τ_x, τ_y, τ_z are elements of Pauli spin-operators used to represent pseudospin. The Fermi velocity in the low-energy region near the Dirac point is $v_F \cong 5.5\times10^5\,\mathrm{m/s}$ [55]. The notation $\Delta_{\eta\sigma} = \eta\sigma\Delta_{SO}$ represents spin-valley-dependent energy gap in NMs regions, where $\Delta_{SO} = 3.9$ meV is effective spin-orbit coupling [104].

On the other hand, the low-energy Hamiltonian in ferromagnetic region FM1 under the effects of electric field, exchange field, and chemical potential can be described as

$$H_{\eta\sigma} = v_F(p_x\tau_x - \eta p_y\tau_y) - \Delta_{\eta\sigma 1}\tau_z - \mu_{\sigma 1}, \tag{4.3}$$

where $\Delta_{\eta\sigma 1} = \eta\sigma\Delta_{SO} - \Delta_E + \sigma\Delta_{M1}$ is spin-valley dependent energy gap, $\Delta_E = eDE_z$ is the energy gap due to electric field, $\Delta_{M1} = (h_{1A} - h_{1B})/2$ is the energy gap induced by exchange field. The spin-dependent chemical potential is defined as $\mu_{\sigma 1} = \mu + \sigma u_{M1}$, where $u_{M1} = (h_{1A} + h_{1B})/2$, since the chemical potential in the barrier is spin-dependent relating to the exchange field.

Then the Hamiltonian in ferromagnetic region FM2 can be described in the same manner as

$$H_{\eta\sigma} = v_F(p_x\tau_x - \eta p_y\tau_y) - \Delta_{\eta\sigma 2}\tau_z - \mu_{\sigma 2}, \tag{4.4}$$

where $\Delta_{\eta\sigma 2} = \eta\sigma\Delta_{SO} - \Delta_E + \sigma\Delta_{M2}$, $\Delta_{M2} = (h_{2A} - h_{2B})/2$, $\mu_{\sigma 2} = \mu + \sigma u_{M2}$, and $u_{M2} = (h_{2A} + h_{2B})/2$.

Solving the Hamiltonian in Equation (4.1) yields the following eigenvalues and wave functions in each region, where the spin-valley currents flow in the x-direction [66].

Eigenvalues:

$$E = +(-)\sqrt{(v_F p)^2 + \Delta_{\eta\sigma}^2} - \mu_\sigma, \tag{4.5}$$

where p is momentum, the sign $+(-)$ represents the band energy of electron and hole, respectively.

Wave functions:

$$\Psi_{NM1} = \left[\begin{pmatrix} 1 \\ A_{\eta\sigma} e^{-i\eta\theta} \end{pmatrix} e^{ik_x x} + r_{\eta\sigma} \begin{pmatrix} 1 \\ -A_{\eta\sigma} e^{i\eta\theta} \end{pmatrix} e^{-ik_x x} \right] e^{ik_{//} y}$$

$$\Psi_{FM1} = \left[a_{\eta\sigma} \begin{pmatrix} 1 \\ B_{\eta\sigma} e^{-i\eta\alpha_1} \end{pmatrix} e^{il_x x} + b_{\eta\sigma} \begin{pmatrix} 1 \\ -B_{\eta\sigma} e^{i\eta\alpha_1} \end{pmatrix} e^{-il_x x} \right] e^{ik_{//} y},$$

$$\Psi_{NM2} = \left[g_{\eta\sigma} \begin{pmatrix} 1 \\ M_{\eta\sigma} e^{-i\eta\beta} \end{pmatrix} e^{im_x x} + f_{\eta\sigma} \begin{pmatrix} 1 \\ -M_{\eta\sigma} e^{i\eta\beta} \end{pmatrix} e^{-im_x x} \right] e^{ik_{//} y},$$

$$\Psi_{FM2} = \left[p_{\eta\sigma} \begin{pmatrix} 1 \\ N_{\eta\sigma} e^{-i\eta\alpha_2} \end{pmatrix} e^{in_x x} + q_{\eta\sigma} \begin{pmatrix} 1 \\ -N_{\eta\sigma} e^{i\eta\alpha_2} \end{pmatrix} e^{-in_x x} \right] e^{ik_{//} y},$$

$$\Psi_{NM3} = \left[t_{\eta\sigma} \begin{pmatrix} 1 \\ A_{\eta\sigma} e^{-i\eta\theta} \end{pmatrix} e^{ik_x x} \right] e^{ik_{//} y}, \tag{4.6}$$

where parameters

$$A_{\eta\sigma} = \frac{E + \eta\sigma\Delta_{SO}}{\sqrt{E^2 - \Delta_{SO}^2}}, \quad B_{\eta\sigma} = \frac{E + \mu_{\sigma1} + \Delta_{\eta\sigma1}}{\sqrt{(E + \mu_{\sigma1})^2 - \Delta_{\eta\sigma1}^2}},$$

$$M_{\eta\sigma} = \frac{E + \eta\sigma\Delta_{SO}}{\sqrt{E^2 - \Delta_{SO}^2}}, \quad N_{\eta\sigma} = \frac{E + \mu_{\sigma2} + \Delta_{\eta\sigma2}}{\sqrt{(E + \mu_{\sigma2})^2 - \Delta_{\eta\sigma2}^2}}. \tag{4.7}$$

Then the wave vectors in x-direction of electron in NMs and FMs regions are described by

$$k_x = \frac{\sqrt{E^2 - \Delta_{SO}^2}\cos\theta}{\hbar v_F}, \quad l_x = \frac{\sqrt{(E + \mu_{\sigma 1})^2 - \Delta_{\eta\sigma 1}^2}\cos\alpha_1}{\hbar v_F},$$

$$m_x = \frac{\sqrt{E^2 - \Delta_{SO}^2}\cos\beta}{\hbar v_F}, \quad n_x = \frac{\sqrt{(E + \mu_{\sigma 2})^2 - \Delta_{\eta\sigma 2}^2}\cos\alpha_2}{\hbar v_F}, \quad (4.8)$$

where θ is the incident angle of electrons at the NM1/FM1 junction, α_1 is the incident angle at FM1/NM2 junction, β is the incident angle at NM2/FM2 junction, and α_2 is the incident angle at FM2/NM3 junction. These incident angles can be calculated via the conservation component in the y-direction as given by

$$k_{//} = \frac{\sqrt{E^2 - \Delta_{SO}^2}\sin\theta}{\hbar v_F} = \frac{\sqrt{(E + \mu_{\sigma 1})^2 - \Delta_{\eta\sigma 1}^2}\sin\alpha_1}{\hbar v_F}$$

$$= \frac{\sqrt{E^2 - \Delta_{SO}^2}\sin\beta}{\hbar v_F} = \frac{\sqrt{(E + \mu_{\sigma 2})^2 - \Delta_{\eta\sigma 2}^2}\sin\alpha_2}{\hbar v_F}. \quad (4.9)$$

Therefore, the coefficients $r_{\eta\sigma}$, $a_{\eta\sigma}$, $b_{\eta\sigma}$, $g_{\eta\sigma}$, $f_{\eta\sigma}$, $p_{\eta\sigma}$, $q_{\eta\sigma}$, $t_{\eta\sigma}$ can be calculated by using the following boundary conditions.

$$\Psi_{NM1}(0) = \Psi_{FM1}(0), \quad \Psi_{FM1}(d) = \Psi_{NM2}(d),$$

$$\Psi_{NM2}(d + L) = \Psi_{FM2}(d + L), \quad \Psi_{FM2}(2d + L) = \Psi_{NM3}(2d + L), \quad (4.10)$$

where $r_{\eta\sigma}$ and $t_{\eta\sigma}$ represent reflection and transmission coefficients, respectively. Using the wave functions in Equation (4.6) and the boundary conditions in Equation (4.10), we can construct a matrix equation as follows:

$$\begin{bmatrix} 1 & -1 & -1 & 0 & 0 & 0 & 0 & 0 \\ -Ae^{i\eta\theta} & -Be^{-i\eta\alpha_1} & Be^{i\eta\alpha_1} & 0 & 0 & 0 & 0 & 0 \\ 0 & e^{il_xd} & e^{-il_xd} & -e^{im_xd} & -e^{-im_xd} & 0 & 0 & 0 \\ 0 & Be^{-i\eta\alpha}e^{il_xd} & -Be^{i\eta\alpha_1}e^{-il_xd} & -Me^{-i\eta\beta}e^{im_xd} & Me^{i\eta\beta}e^{-im_xd} & 0 & 0 & 0 \\ 0 & 0 & 0 & e^{im_x(d+L)} & e^{-im_x(d+L)} & -e^{in_x(d+L)} & -e^{-in_x(d+L)} & 0 \\ 0 & 0 & 0 & Me^{-i\eta\beta}e^{im_x(d+L)} & -Me^{i\eta\beta}e^{-im_x(d+L)} & -Ne^{-i\eta\gamma}e^{in_x(d+L)} & Ne^{i\eta\gamma}e^{-in_x(d+L)} & 0 \\ 0 & 0 & 0 & 0 & 0 & e^{in_x(2d+L)} & e^{-in_x(2d+L)} & -e^{ik_x(2d+L)} \\ 0 & 0 & 0 & 0 & 0 & Ne^{-i\eta\alpha_2}e^{in_x(2d+L)} & -Ne^{i\eta\alpha_2}e^{-in_x(2d+L)} & -Ae^{-i\eta\theta}e^{ik_x(2d+L)} \end{bmatrix} \begin{bmatrix} r \\ a \\ b \\ g \\ f \\ p \\ q \\ t \end{bmatrix} = \begin{bmatrix} -1 \\ -Ae^{-i\eta\theta} \\ 0 \\ 0 \\ 0 \\ 0 \\ 0 \\ 0 \end{bmatrix}$$

The above matrix equation can be solved to find $t_{\eta\sigma}$ by using Cramer's rule explained in Chapter 3 with the help of Mathematica. Then the transmission probability amplitude $T_{\eta\sigma}$ could be calculated with the formula $T_{\eta\sigma} = J_t / J_{in} = |t_{\eta\sigma}|^2$, where J_t is the current density of transmitted electrons and J_{in} is the current density of injected electrons, respectively. With the transmission probability amplitude $T_{\eta\sigma}$, the spin-valley conductance at the temperature of zero Kelvin in ballistic regime can be calculated by using the standard Landauer's formalism and integrating the whole incident angles [105, 106] as

$$G_{\eta\sigma} = \frac{e^2}{h} N(E) |t_{\eta\sigma}|^2 = G_0 \frac{\sqrt{E^2 - \Delta_{SO}^2}}{|E|} \int_{-\pi/2}^{\pi/2} \frac{1}{8} d\theta \cos(\theta) T_{\eta\sigma} . \qquad (4.11)$$

The notation $G_0 = \frac{4e^2}{h} N_0(E)$ represents unit conductance, $N_0(E) = \frac{W}{\pi\hbar v_F} |E|$ is the density of state in the transport channel of electrons in silicene when the spin-orbit interaction effect is excluded. W is the width of silicene sheet, h represents Planck's constant, and $N(E) = \frac{W}{\pi\hbar v_F}\sqrt{E^2 - \Delta_{SO}^2}$ is the density of state in the transport channel of electrons in normal silicene junction.

From Equation (4.10), the total conductance G_T could be calculated with the summation of all spin-valley conductances as

$$G_T = G_{k\uparrow} + G_{k\downarrow} + G_{k'\uparrow} + G_{k'\downarrow}, \qquad (4.12)$$

where $\eta=+1$ represents k, $\eta=-1$ represents k', $\sigma=+1$ represents spin ↑, and $\sigma=-1$ represents spin ↓. Furthermore, the spin polarization (SP) and valley polarization (VP) can be defined as

$$SP(\%) = \frac{(G_{k\uparrow} + G_{k'\uparrow}) - (G_{k\downarrow} + G_{k'\downarrow})}{G_T} \times 100 \,,$$

$$VP(\%) = \frac{(G_{k\uparrow} + G_{k\downarrow}) - (G_{k'\uparrow} + G_{k'\downarrow})}{G_T} \times 100 \,. \tag{4.13}$$

Unlike SP and VP, the sublattice pseudospin polarization (PP) is more difficult to define intuitively. Therefore, we use quantum mechanics to define sublattice pseudospin polarization. The expectation value of sublattice-pseudospin [107, 108] is defined by quantum mechanics as

$$\langle \vec{s} \rangle_{\eta\sigma} = \left\langle \Psi_{\eta\sigma} \left| \hat{\vec{s}} \right| \Psi_{\eta\sigma} \right\rangle, \tag{4.14}$$

where $\Psi_{\eta\sigma} = \begin{pmatrix} \Psi_{A,\eta\sigma} \\ \Psi_{B,\eta\sigma} \end{pmatrix}$ is the normalized wave function of electrons. Then the sublattice pseudospin operator may be defined as

$$\hat{\vec{s}} = \frac{\hbar}{2}(\tau_x \hat{a}_x + \tau_y \hat{a}_y + \tau_z \hat{a}_z). \tag{4.15}$$

Therefore, the expectation value is described as

$$\langle \vec{s} \rangle_{\eta\sigma} = \frac{\hbar}{2}\left(\sqrt{1 - \left(\frac{\Delta_{so}}{E}\right)^2} \, \hat{a}_{xy} - \eta\sigma \frac{\Delta_{so}}{E} \hat{a}_z \right), \tag{4.16}$$

where $\hat{a}_{xy}$ is a unit vector in xy-plane and $\hat{a}_z$ is a unit vector in z-direction. When $E \to \Delta_{SO}$, the expectation value can be approximated as

$$\langle \vec{s} \rangle_{\eta\sigma} \to -\eta\sigma \frac{\hbar}{2} \hat{a}_z. \tag{4.17}$$

With the limit $E \rightarrow \Delta_{SO}$, we can separate electrons in silicene into two sublattice-pseudospin groups as

$$\langle \vec{s} \rangle_{k\uparrow} = \langle \vec{s} \rangle_{k'\downarrow} = -\frac{\hbar}{2}\hat{a}_z ,$$ (4.18)

which represents the state of sublattice-B or sublattice-pseudospin down $|\Downarrow\rangle$, and

$$\langle \vec{s} \rangle_{k\downarrow} = \langle \vec{s} \rangle_{k'\uparrow} = +\frac{\hbar}{2}\hat{a}_z,$$ (4.19)

which represents the state of sublattice-A or sublattice-pseudospin up $|\Uparrow\rangle$. In summary the state of sublattice-pseudospin down $|\Downarrow\rangle$ is the states of $|k\uparrow\rangle$ and $|k'\downarrow\rangle$, while the state of sublattice-pseudospin up $|\Uparrow\rangle$ is the states of $|k\downarrow\rangle$ and $|k'\uparrow\rangle$.

Therefore, the sublattice pseudospin polarization (PP) in silicene can be considered as a polarization that occurs when $E \rightarrow \Delta_{SO}$, where it can be defined as [71]

$$PP(\%) = \frac{(G_\Uparrow - G_\Downarrow)}{G_T} \times 100 = \frac{(G_{k\downarrow} + G_{k'\uparrow}) - (G_{k\uparrow} + G_{k'\downarrow})}{G} \times 100 .$$ (4.20)

The notation $G_\Uparrow = G_{k\downarrow} + G_{k'\uparrow}$ is conductance of electrons with sublattice pseudospin up, and $G_\Downarrow = G_{k\uparrow} + G_{k'\downarrow}$ is conductance of electrons with sublattice pseudospin down, respectively.

4.2.2 The Basic Structure with a Middle Gate

To further analyze the impact of interplay between electric fields and exchange field configurations on the spin-valley polarized currents in the proposed dual ferromagnetic-gated silicene junctions, another gate potential *U/e* is also applied to the silicene in NM2 region. The modified device structure is shown in Figure 4-2. The low-energy effective Hamiltonian of this structure is almost the

same as in the structure without gate potential *U/e* shown in Figure 4-1, except the change in the parameters of Equation (4.7) which becomes

$$A_{\eta\sigma} = \frac{E + \eta\sigma\Delta_{SO}}{\sqrt{E^2 - \Delta_{SO}^2}}, \quad B_{\eta\sigma} = \frac{E + \mu_{\sigma1} + \Delta_{\eta\sigma1}}{\sqrt{(E + \mu_{\sigma1})^2 - \Delta_{\eta\sigma1}^2}},$$

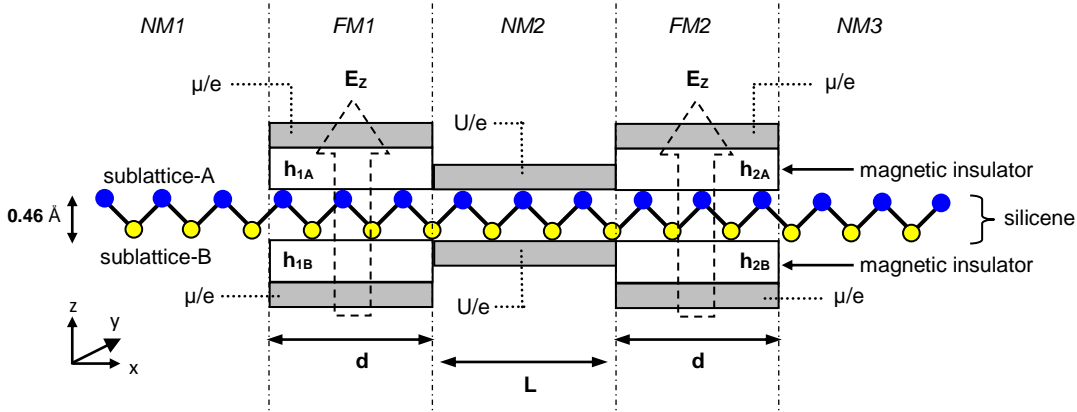$$M_{\eta\sigma} = \frac{E + U + \eta\sigma\Delta_{SO}}{\sqrt{(E + U)^2 - \Delta_{SO}^2}}, \quad N_{\eta\sigma} = \frac{E + \mu_{\sigma2} + \Delta_{\eta\sigma2}}{\sqrt{(E + \mu_{\sigma2})^2 - \Delta_{\eta\sigma2}^2}}. \qquad (4.21)$$

Figure 4-2: Schematic model of proposed structure with additional gate potential U/e at NM2 region.

In addition, the wave vectors in *x*-direction of electrons in NMs and FMs regions in Equation (4.8) becomes

$$k_x = \frac{\sqrt{E^2 - \Delta_{SO}^2}\,\cos\theta}{\hbar v_F}, \quad l_x = \frac{\sqrt{(E + \mu_{\sigma1})^2 - \Delta_{\eta\sigma1}^2}\,\cos\alpha_1}{\hbar v_F},$$

$$m_x = \frac{\sqrt{(E + U)^2 - \Delta_{SO}^2}\,\cos\beta}{\hbar v_F}, \quad n_x = \frac{\sqrt{(E + \mu_{\sigma2})^2 - \Delta_{\eta\sigma2}^2}\,\cos\alpha_2}{\hbar v_F}, \qquad (4.22)$$

while the other formulas stay the same as in the case of the structure without a gate on NM2 region.

4.3 Results and Discussion

We show the analysis results and discuss the results in this section. The dimension of the device structure is set to be gate width $d = 25$ nm, and the gap between gate $L = 25$ nm. The excited energy of electrons is designated to be $E = 4$ meV. The four configurations of magnetic exchange fields used in our analysis are illustrated in Figure 4-3, where the exchange field magnitude is $h = 5$ meV. Throughout this analysis, we set the parameter d, L, E, and h to be fixed at the same values.
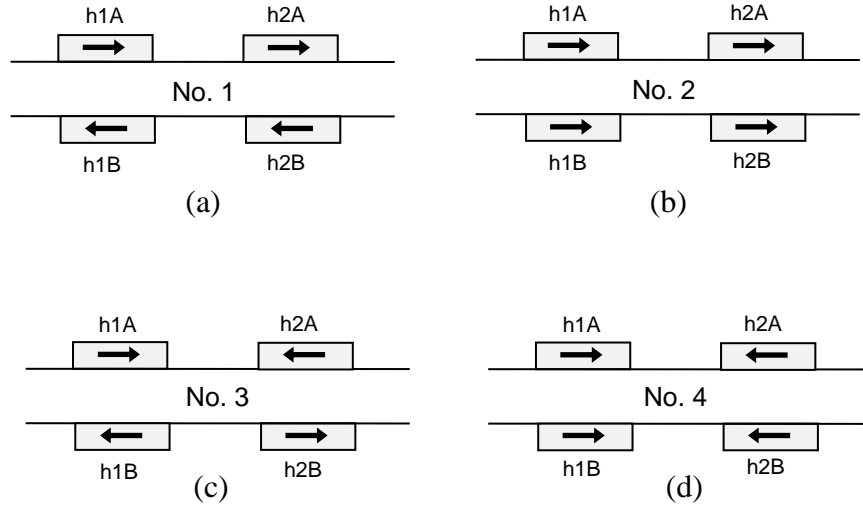
Figure 4-3: Configurations of magnetic exchange fields, where $\rightarrow$ represents h, and $\leftarrow$ represents $-h$. (a) configuration No.1, (b) configuration No.2, (c) configuration No.3, (d) configuration No.4.

The reason that we designated the excited energy to be $E = 4$ meV is because we would like to investigate the electronic transport occurring at the bottom of the energy band. In that system, the low-energy Hamiltonian could be realized because of the $E \cong \Delta_{SO}$. At the low energy region, many intriguing phenomena occur due to the fact that the electrons in that region obey Dirac equation, and this is the focus area of our investigation. One interesting phenomenon is that the effect of spin-valley dependent energy gap in the barriers

is strong in the system of $E \cong \Delta_{SO}$ [66]. In our analysis, we particularly look at the conductance of electrons and the polarization of the spin currents, valley currents as well as sublattice pseudospin currents. We systematically analyze the impact of exchange field configurations, external electric field, and middle gate bias on the behavior of electronic transport. Figure 4-4 shows the normalized conductance of each spin-valley current component as a function of external electric field E_z, where e is elementary charge and D is the perpendicular distance between sublattice-A and sublattice-B. In this case, the chemical potential is set to be $\mu = 0$ meV without middle gate bias.
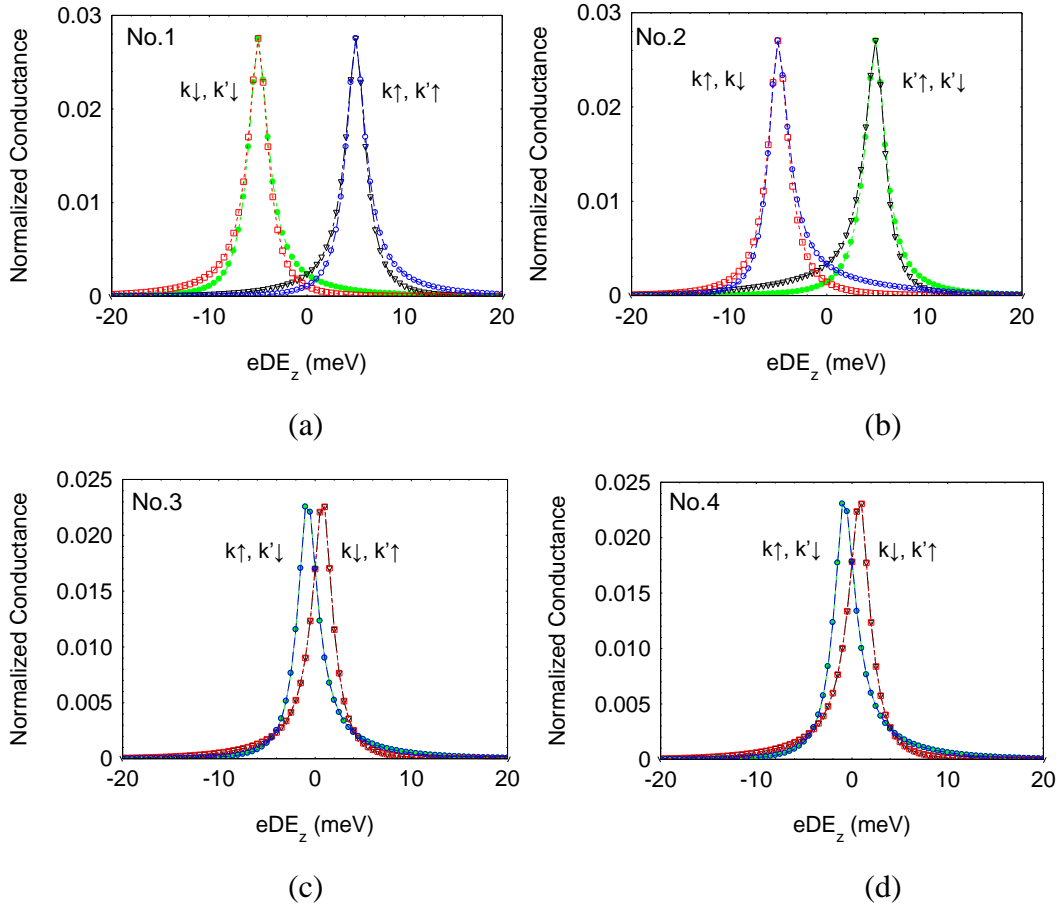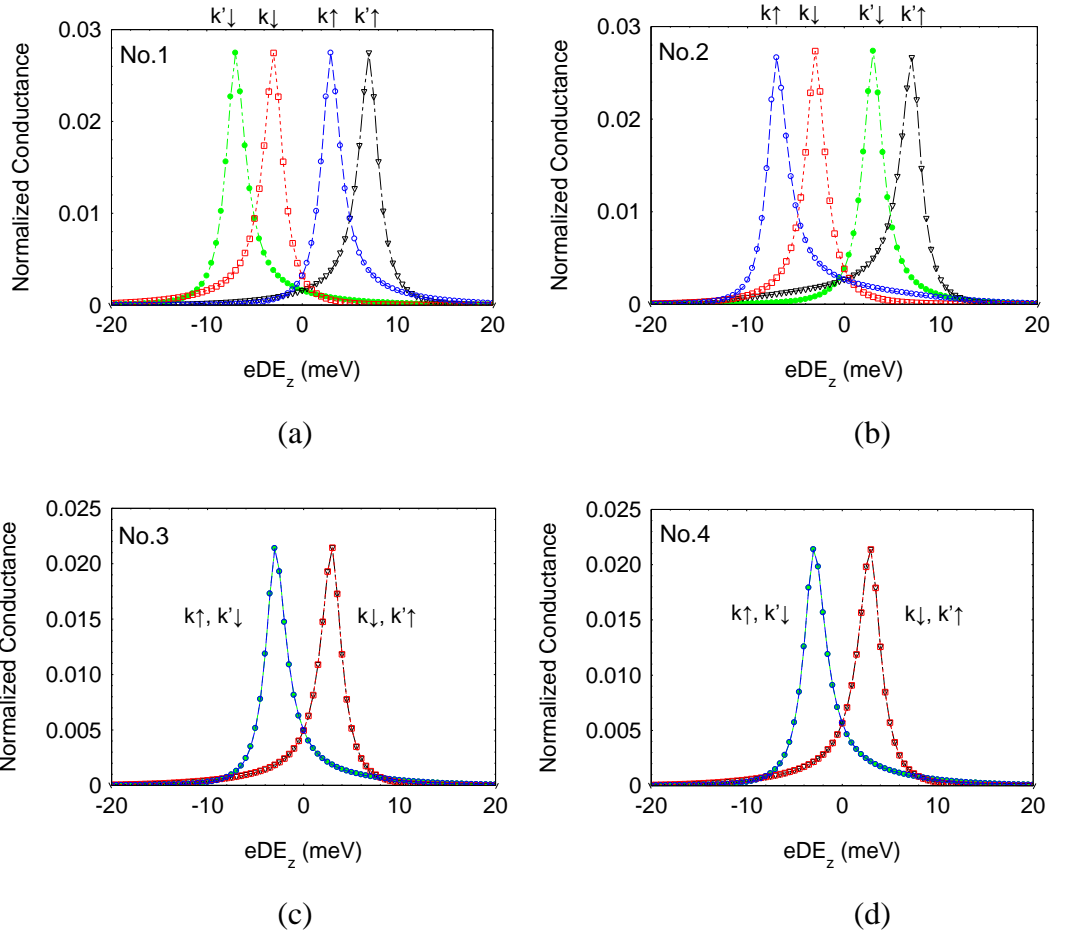

Figure 4-4: Conductance as the function of electric field with chemical potential μ = 0 meV in exchange field configuration (a) No.1, (b) No.2, (c) No.3, and (d) No.4.

Figure 4-4(a) exhibits perfect spin polarization of almost 100% at $eDE_z = \pm h$ meV in exchange field configuration No.1. Pure spin current can be controlled to flip between spin up and spin down by reversing the direction of

electric field. On the other hand, the Figure exhibits valley polarization at $eDE_z = 0$ meV, where $G_{k\uparrow} = G_{k\downarrow}$ and $G_{k'\uparrow} = G_{k'\downarrow}$. On the contrary, Figure 4-4(b) exhibits perfect valley polarization of almost 100% at $eDE_z = \pm h$ meV in exchange field configuration No.2, while exhibits spin polarization at $eDE_z = 0$ meV, where $G_{k\uparrow} = G_{k'\uparrow}$ and $G_{k\downarrow} = G_{k'\downarrow}$. Figure 4-4(c) and Figure 4-4 (d) exhibit similar characteristics with both spin polarization and valley polarization disappear in exchange field configuration No.3 and No.4. They show sublattice pseudospin polarization near $eDE_z = 0$.
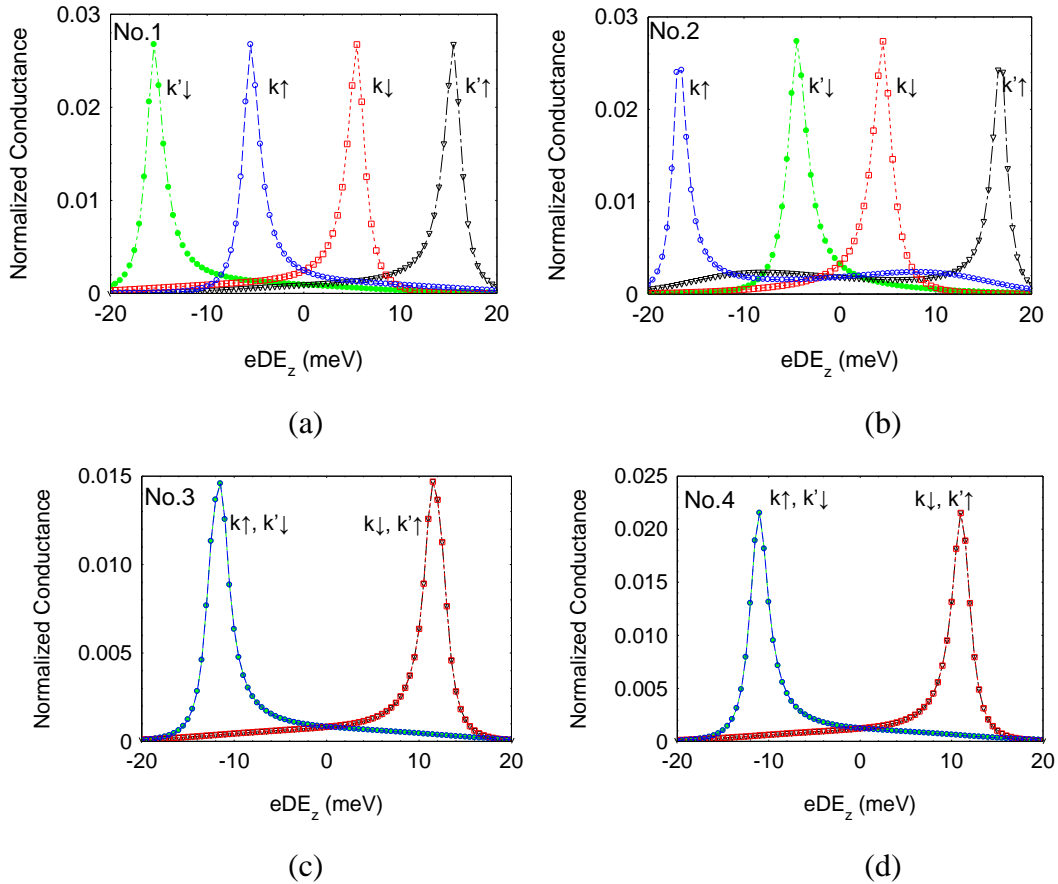

Figure 4-5: Conductance as the function of electric field with chemical potential μ = 2.0 meV in exchange fields configuration (a) No.1, (b) No.2, (c) No.3, and (d) No.4.

Figure 4-5(a) and (b) show similar characteristics of perfect spin-valley polarization in exchange field configuration No.1 and No.2. The result is similar to what was reported in a single ferromagnetic gated silicene junction [66]. The distance between peaks may be adjusted by varying chemical potential μ. Figure

4-5(c) and (d) exhibit sublattice pseudospin polarization similar to that in Figure 4-4(c) and (d) with wider splitting. The peaks splitting can be enhanced even further in all exchange field configurations by applying middle gate bias as illustrated in Figure 4-6. This result is meaningful for applications in perfect spin-valley filtering and sublattice pseudospin filtering devices. The study results also indicate that the device structure with exchange field configuration No.1 and No.2 may function as a spin polarizer and a valley polarizer, respectively. On the other hand, the device structure with exchange field configuration No.3 and No. 4 may work as a sublattice pseudospin polarizer.

Figure 4-6: Conductance as the function of electric field with chemical potential μ = 2.0 meV and middle gate bias U = 100 meV in exchange fields configuration (a) No.1, (b) No.2, (c) No.3, and (d) No.4.

Figure 4-7 illustrates effects of middle gate bias U on the spin and valley polarization in exchange field configuration No.1 and No. 2. When the external electric field E_z = 0 meV and chemical potential μ = 0 meV, the structure exhibits pure valley polarization in configuration No.1 and exhibits pure spin polarization

in configuration No. 2 as shown in Figure 4-4(a) and (b). It was found that the pure valley polarization, where only $VP \neq 0$ while $SP = LSP = 0$, can be controlled to switch from -100% to almost 100% by increasing the middle gate bias U in configuration No. 1 as illustrated in Figure 4-7(a). On the other hand, Figure 4-7(b) depicts the control of pure spin polarization, where only $SP \neq 0$ and $VP = LSP = 0$, to switch from 100% to almost -100% by increasing the middle gate bias U in configuration No. 2. Figure 4-8(a) and (b) show similar characteristics control of spin polarization and valley polarization by chemical potential μ when the external electric field $E_z = 0$ meV and middle gate bias $U = 0$ meV in configuration No.1 and No.2, respectively. The oscillation of valley polarization and spin polarization in Figure 4-7 and Figure 4-8 is due to the quantum interference of electrons in the barriers, where the period of oscillation may decrease as the barrier thickness increases.
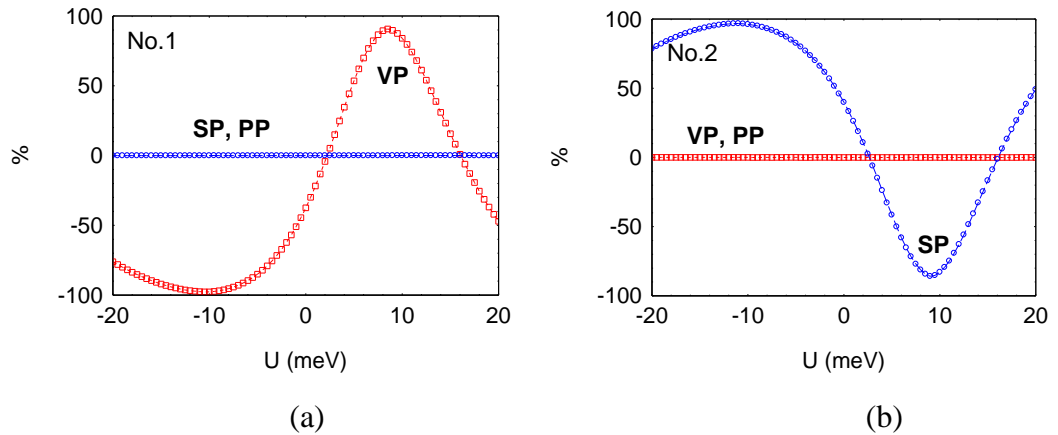

(a)   (b)

Figure 4-7: Spin polarization (SP), valley polarization (VP), and pseusospin polarization (PP) as the function of middle gate bias U with the external electric field E_z=0 meV and chemical potential $\mu = 0$ meV in configuration (a) No.1, (b) No.2.
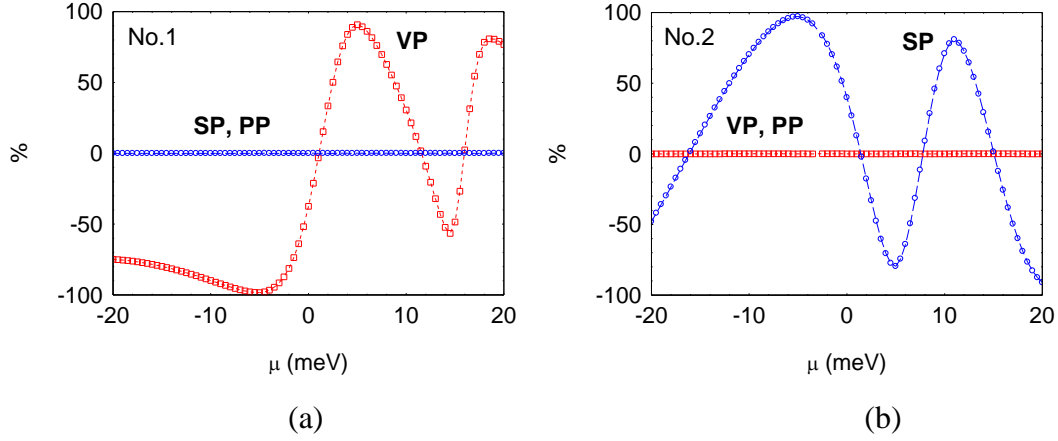
Figure 4-8: Spin polarization (SP), valley polarization (VP), and pseusospin polarization (PP) as the function of chemical potential μ with the external electric field E_z=0 meV and middle gate bias $U = 0$ meV in configuration (a) No.1, (b) No.2.

From Figure 4-4 to Figure 4-6, we have seen that the device structure with exchange field configuration No.3 and No.4 behave as a sublattice pseudospin polarizer. Our investigation results show in Figure 4-9 that the pseudospin polarization can be controlled to switch from almost -100% to almost 100% by increasing the external electric field eDE_z. Particularly when the middle gate bias $U = 100$ meV, the pseudospin polarization fully switch from -100% to 100% linearly in both exchange field configurations. The spin polarization and valley polarization are 0 % under this condition, which indicates pure pseudospin polarization. The results show a promising characteristic for applications in silicene-based pseudospintronics.

The abovementioned results are discussed here. The conductance of the junction is determined by the transmission probability amplitude as seen in Equation (4.11). This might be intuitively understood as high conductance occurs when the transmission probability is high. On the other hand, the transmission probability is determined by how well electrons can transport through the barriers, which depends on the positions of conduction bands and the width of the band gap [66].
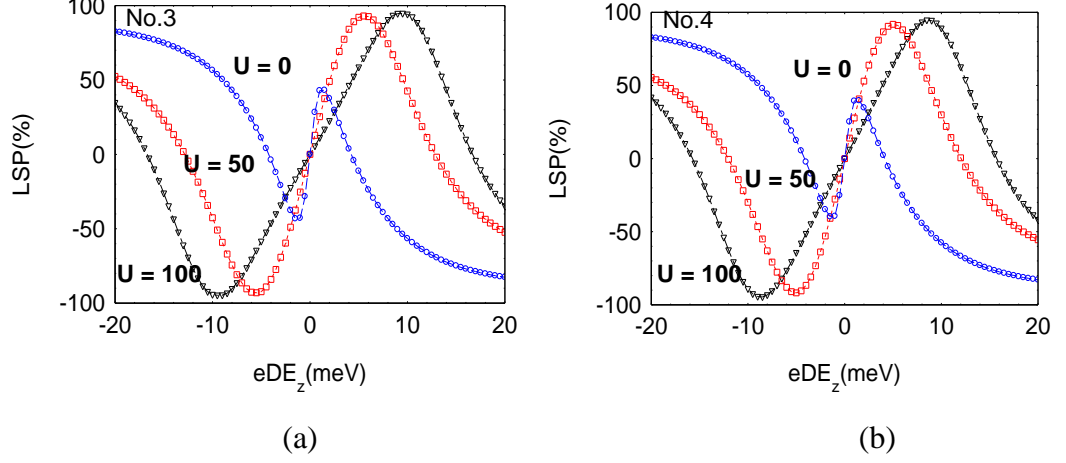
Figure 4-9: Lattice-pseudospin polarization as the function of electric field with chemical potential $\mu = 2.5$ meV and varied middle gate $U = 0, 50, 100$ meV in exchange fields configuration (a) No.1, (b) No.2.

In general, the width of the band gap at the ferromagnetic barrier without light irradiation is determined by spin-valley dependent energy gap $\Delta_{\eta\sigma} = \eta\sigma\Delta_{SO} - \Delta_E + \sigma\Delta_M$ of which each spin-valley component is different among each other. For instance, the index of $k\uparrow$ is $\eta = +1$, $\sigma = +1$. In the same manner, the index of $k'\uparrow$ is $\eta = -1$, $\sigma = +1$, $k\downarrow$ is $\eta = +1$, $\sigma = -1$, and $k'\downarrow$ is $\eta = -1$, $\sigma = -1$. Therefore, the spin-valley dependent energy gap for each current component is

$$\Delta_{k\uparrow} = \Delta_{SO} - \Delta_E + \Delta_M ,$$

$$\Delta_{k'\uparrow} = -\Delta_{SO} - \Delta_E + \Delta_M ,$$

$$\Delta_{k\downarrow} = -\Delta_{SO} - \Delta_E - \Delta_M ,$$

$$\Delta_{k'\downarrow} = \Delta_{SO} - \Delta_E - \Delta_M . \tag{4.23}$$

On the other hand, the width of the band gap at the normal region NMs with light irradiation is determined by spin-valley dependent energy gap $\Delta_{\eta\sigma} = \eta\sigma\Delta_{SO} + \eta\lambda_\Omega$. The interplay between electric field induced energy gap Δ_E,

45

exchange field induced energy gap Δ_M, and spin-orbit coupling Δ_{SO} causes changes on the band gap, which in turn affects the transmission probability amplitude of each spin-valley component in different way. In addition, the spin-dependent chemical potential $\mu_\sigma = \mu + \sigma u_M$ and the middle gate potential U/e also affect the low-energy Hamiltonian and wave functions as illustrated in Equation (4.4), (4.6), (4.7), (4.8), (4.9), (4.21), and (4.22).

It is also worth noting here that the magnitudes of normalized conductance illustrated from Figure 4-4 to Figure 4-6 are less than 0.03, which is a very small number. The reason of small conductance magnitude is due to the exciting energy level that we use in this theoretical analysis. From Equation (4.10), when the excited energy $E = 4$ meV approaches $\Delta_{SO} = 3.9$ meV, which is in the energy range we are interested in, so that fewer density of states are available in transport channel.

4.4 Conclusions

In this section we have investigated the electronic transport properties in dual ferromagnetic-gated silicene junction under the influences of external electric field, magnetic exchange field, chemical potential, and optional middle gate bias. The magnetic exchange fields, which are induced into two ferromagnetic regions by proximity effects, are arranged into four configurations to see the effects on the electronic transport properties in the device structure. The numerical analysis results show that, in the absence of chemical potential μ, the junction might behave as either pure spin polarizer or pure valley polarizer depending on the direction of exchange fields No.1 or No.2. Interestingly, when the exchange field configuration is arranged to No.3 and No.4, the pure and perfect spin-valley polarization characteristics are broken to yield a pure sublattice pseudospin polarization. On the other hand, the junction exhibits perfect spin-valley polarization in exchange field configuration No.1 and No.2, while the distance between peaks is widened in configuration No.3 and No.4, when chemical potential μ is applied. The results depict similar characteristics as in the single ferromagnetic-gated junctions. We also found that the peaks splitting effect is

enhanced in all exchange field configurations, when a middle gate bias U is applied.

The pseudospin polarization can be controlled by electric field. In particular, it can be linearly controlled from -100% to 100% when an appropriate middle gate bias U is applied. In other words, the polarized currents in the junction with exchange field configuration No.3 and No.4 can be controlled to flow only in sublattice-A or sublattice-B when PP= $+100\%$ or -100%, respectively. This perfectly controllable sublattice pseudospin current in silicene was found only in dual ferromagnetic-gated junctions, and is not achievable in single ferromagnetic-gated junctions.

Chapter 5

Photo-Irradiation Effects

We have investigated the electronic transport properties in a dual ferromagnetic-gated silicene junction in Chapter 4. The analysis results show that in the absence of chemical potential μ, the junction might behave as either pure spin polarizer, pure valley polarizer, or pure sublattice pseudospin polarization depending on the exchange field configuration. On the other hand, the junction might exhibit perfect spin-valley polarization or just widen the distance between peaks depending on the exchange field configuration, when chemical potential is applied. In this section we investigate the electronic transport properties of the same device structure when circularly polarized photo irradiation is applied to the NM2 region, while there are electric fields and chemical potentials applied to the gates. We also look at the tunnel magnetoresistance (TMR) characteristics. Tunnel magnetoresistance is an interesting phenomenon which is widely applied to many types of devices such as read heads of hard disk drive, magnetoresistive random-access memory (MRAM), and sensing applications.

5.1 Introduction

Photo-induced effect is one topic that attracts attention in silicene research due to the similar study in graphene, where circularly polarized light is used to open a gap at the Dirac point [72]. In silicene, there is a study reported that the topological class of silicene could be changed from quantum spin-Hall insulator (QSHI) to other phase which has different properties by irradiation of circularly polarized light under the influence of electric field [73]. It is reported that off-resonant circularly polarized light irradiation on silicene has effects on the band structure due to photon dressing effect. In this scheme, spin-valley polarization

depends on the intensity of light, and electric field. The spin-valley polarization can also be inverted by reversing the direction of electric field or the circular polarization of the light [75]. It was discovered that spin-valley polarizations and tunnel magnetoresistance in a ferromagnetic-normal-ferromagnetic junction can be significantly enhanced by photo irradiation on one of ferromagnetic gates without influence of electric field or magnetic field [76]. There is also a study in effective photo-induced band structure manipulation with intense terahertz irradiation beyond the off-resonant condition [77]. However, there has been no investigation on the impact of the photo irradiation to the normal region between gates in a dual ferromagnetic-gated silicene junction with electric field and exchange field at two ferromagnetic gates.

5.2 Circularly Polarized Light and Photon Dressing

According to the electromagnetic theory, light is an electromagnetic wave in which a magnetic field intertwines with an electric field in the same space. The electric field vectors in the electromagnetic wave lie in a plane perpendicular to that of the magnetic field vectors as well as perpendicular to the direction of the wave propagation. However, there is no specific plane of the electric field vectors and magnetic field vectors. The plane may also change over the time, and this is called unpolarized light or nature light.

On the other hand, the light which has the plane of the electric field vectors and magnetic field vectors fixed is called linear polarized light. Another kind of polarized light is called circularly polarized light, of which the plane of the electric field vectors and magnetic field vectors rotates [109]. The circularly polarized light can be either right-handed (clockwise) or left-handed (counterclockwise) depending on the direction of rotation. In other words, circularly polarized light is the light that has a constant magnitude of electric field while rotating at a steady rate in a plane perpendicular to the direction of the light as illustrated in Figure 5-1. The polarized light is not necessary a special characteristic of visible light. Other electromagnetic waves, such as x-rays and radio wave, may also be polarized.
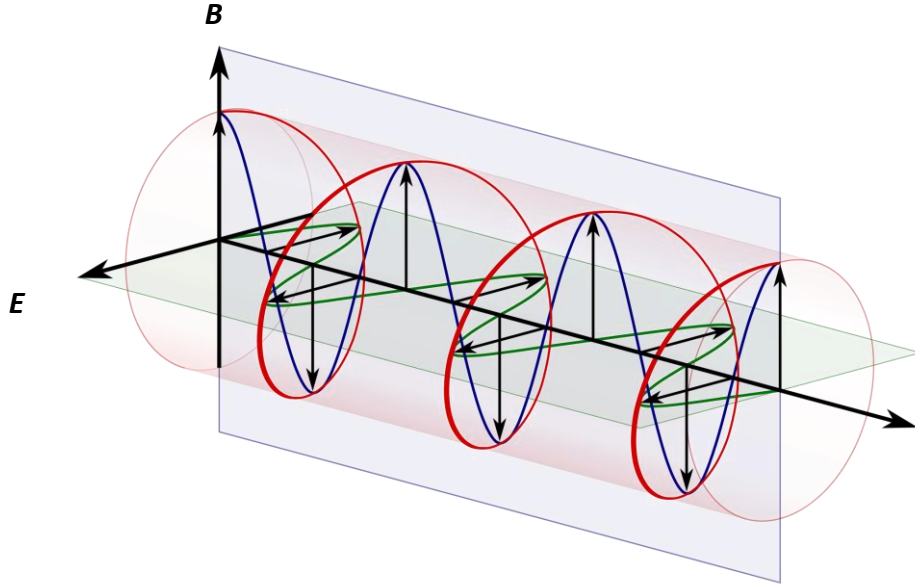
Figure 5-1: Illustration of circularly polarized light [110].

Photon dressing is the interaction between photons and electrons in nanoscale, which causes a new phase of electronic structure [111]. The interaction results in quasiparticles of combined photons and electrons with a distinct Floquet-Bloch band structure [112]. When light with off-resonant frequency is irradiated to a matter, the light energy would not be absorbed by electronic states of the matter. The photon energy instead dresses the electronic states via virtual photon processes. Because electronic states are affected or dressed by the photon, we call this interaction photon dressing, which gives rise to new electronic states with different properties.

5.3 Device Models

The device being used in our investigation has the same structure as that in Section 4 without middle gate as shown in Figure 5-2. Controllable perpendicular electric fields E_Z are applied to both ferromagnetic barriers with the same magnitude. Since the effect of spin-valley dependent energy gap in the barriers is strong when the excited energy $E \cong \Delta_{SO}$. This scheme results in resonant conductance peaks as a spin-valley filter [66]. Therefore we focus on this regime to investigate spin-valley filtering effect induced by frequency of polarized photon.

Circularly polarized light $A(t) = A_0(\sin(\Omega t), \cos(\Omega t))$ is irradiated to the NM2 region between ferromagnetic gates, where Ω is light frequency, $A(t)$ is time-dependent vector potential of photon, and A_0 is light magnitude. The off-resonant light frequency used in our investigation is the frequency region where the electronic band structures are changed by virtual photon absorption processes in which there is no direct electrons excitation. In the π-band tight-binding model, this scheme can be achieved when $\hbar|\Omega| \gg t_0$, where t_0 is the nearest hopping energy. The lowest frequency Ω that satisfies this condition can be obtained from the bandwidth where $3t_0 = 4.8$ eV $= 10^{15}$ Hz [73]. In this study, we investigate two magnetic exchange field configurations: parallel junction (P) which is the configuration No. 2 in Chapter 4 where $h_{1A} = h_{1B} = h_{2A} = h_{2B} = 5$ meV, and anti-parallel junction (AP) which is a new configuration where $-h_{1A} = h_{1B} = -h_{2A} = h_{2B} = 5$ meV.

Tight-binding model is used to define low-energy effective Hamiltonians, which are used to describe the electronic transport in this investigation in the same manner as in Chapter 4. The Hamiltonians for the ferromagnetic regions FM1 and FM2 are defined respectively as

$$H_{\eta\sigma} = v_F(p_x\tau_x - \eta p_y\tau_y) - \Delta_{\eta\sigma1}\tau_z - \mu_{\sigma1}$$

$$H_{\eta\sigma} = v_F(p_x\tau_x - \eta p_y\tau_y) - \Delta_{\eta\sigma2}\tau_z - \mu_{\sigma2}, \tag{5.1}$$
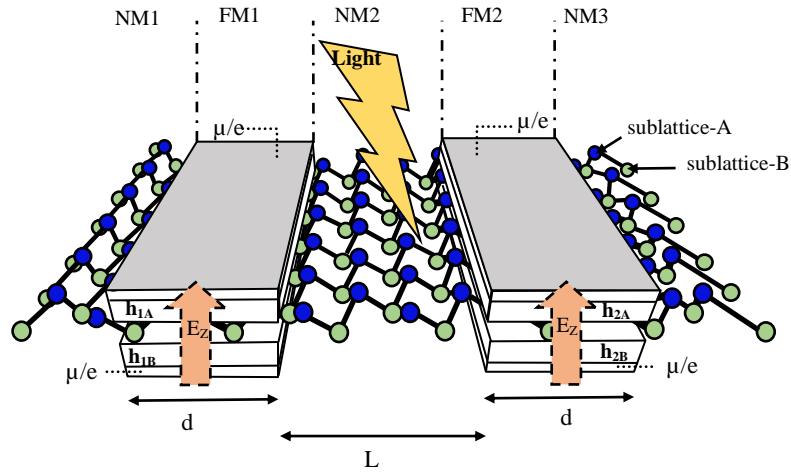

Figure 5-2: Schematic model of proposed structure NM1/FM1/NM2/FM2/NM3 with light irradiation.

The notations k and k' valley is represented with $\eta = +1$ and $\eta = -1$, while spin $\uparrow$ and $\downarrow$ is represented with $\sigma = +1$ and $\sigma = -1$, respectively. Spin-valley dependent energy gaps are $\Delta_{\eta\sigma1} = \eta\sigma\Delta_{SO} - \Delta_E + \sigma\Delta_{M1}$ and $\Delta_{\eta\sigma2} = \eta\sigma\Delta_{SO} - \Delta_E + \sigma\Delta_{M2}$, where electric field-induced energy gap is $\Delta_E = eDE_z$, and the exchange field-induced energy gaps are $\Delta_{M1} = \dfrac{(h_{1A} - h_{1B})}{2}$, $\Delta_{M2} = \dfrac{(h_{2A} - h_{2B})}{2}$. The spin-dependent chemical potentials could be defined with $\mu_{\sigma1} = \mu + \sigma u_{M1}$ and $\mu_{\sigma2} = \mu + \sigma u_{M2}$, where $u_{M1} = (h_{1A} + h_{1B})/2$ and $u_{M2} = (h_{2A} + h_{2B})/2$, respectively.

The Hamiltonian in normal region NM2 with photo irradiation can be described as

$$H_{\eta\sigma} = v_F(p_x\tau_x - \eta p_y\tau_y) - \Delta_{\eta\sigma}\tau_z, \tag{5.2}$$

where Spin-valley dependent energy gap is $\Delta_{\eta\sigma} = \eta\sigma\Delta_{SO} + \eta\lambda_\Omega$, and $\lambda_\Omega = (e\Lambda V_F)^2/\hbar\Omega$. We use $\Lambda = eA_0 a/\hbar$ which is a dimensionless number to characterize the light intensity with e represents the elementary charge, A_0 represents the magnitude of light wave, and a represents the lattice constant of silicene [72, 76]. The value of Λ is generally less than 1 for the intensity from light sources in the frequency range of our interest [73].

In the normal regions NM1 and NM3, where there is neither photo irradiation nor external electric field, the spin-valley dependent energy gap is $\Delta_{\eta\sigma3} = \eta\sigma\Delta_{SO}$. Therefore, the Hamiltonian in these two regions could be defined as

$$H_{\eta\sigma} = v_F(p_x\tau_x - \eta p_y\tau_y) - \eta\sigma\Delta_{so}\tau_z. \tag{5.3}$$

Solving the Hamiltonians, when the spin-valley currents flow in the x-direction, yields the wave function in each region as follows:

$$\Psi_{NM1} = \left[\begin{pmatrix} 1 \\ A_{\eta\sigma}e^{-i\eta\theta} \end{pmatrix} e^{ik_x x} + r_{\eta\sigma} \begin{pmatrix} 1 \\ -A_{\eta\sigma}e^{i\eta\theta} \end{pmatrix} e^{-ik_x x} \right] e^{ik_{//} y}$$

$$\Psi_{FM1} = \left[a_{\eta\sigma} \begin{pmatrix} 1 \\ B_{\eta\sigma} e^{-i\eta\alpha_1} \end{pmatrix} e^{il_x x} + b_{\eta\sigma} \begin{pmatrix} 1 \\ -B_{\eta\sigma} e^{i\eta\alpha_1} \end{pmatrix} e^{-il_x x} \right] e^{ik_{//}y}$$

$$\Psi_{NM2} = \left[g_{\eta\sigma} \begin{pmatrix} 1 \\ M_{\eta\sigma} e^{-i\eta\beta} \end{pmatrix} e^{im_x x} + f_{\eta\sigma} \begin{pmatrix} 1 \\ -M_{\eta\sigma} e^{i\eta\beta} \end{pmatrix} e^{-im_x x} \right] e^{ik_{//}y}$$

$$\Psi_{FM2} = \left[p_{\eta\sigma} \begin{pmatrix} 1 \\ N_{\eta\sigma} e^{-i\eta\alpha_2} \end{pmatrix} e^{in_x x} + q_{\eta\sigma} \begin{pmatrix} 1 \\ -N_{\eta\sigma} e^{i\eta\alpha_2} \end{pmatrix} e^{-in_x x} \right] e^{ik_{//}y}$$

$$\Psi_{NM3} = \left[t_{\eta\sigma} \begin{pmatrix} 1 \\ A_{\eta\sigma} e^{-i\eta\theta} \end{pmatrix} e^{ik_x x} \right] e^{ik_{//}y} , \tag{5.4}$$

where parameters

$$A_{\eta\sigma} = \frac{E + \eta\sigma\Delta_{SO}}{\sqrt{E^2 - \Delta_{SO}^2}} , \quad B_{\eta\sigma} = \frac{E + \mu_{\sigma1} + \Delta_{\eta\sigma1}}{\sqrt{(E + \mu_{\sigma1})^2 - \Delta_{\eta\sigma1}^2}}$$

$$M_{\eta\sigma} = \frac{E + \Delta_{\eta\sigma}}{\sqrt{E^2 - \Delta_{\eta\sigma}^2}} , \text{ and } N_{\eta\sigma} = \frac{E + \mu_{\sigma2} + \Delta_{\eta\sigma2}}{\sqrt{(E + \mu_{\sigma2})^2 - \Delta_{\eta\sigma2}^2}} \tag{5.5}$$

Then the wave vectors in x-direction of electron in NMs and FMs regions are described by

$$k_x = \frac{\sqrt{E^2 - \Delta_{SO}^2} \cos\theta}{\hbar v_F} , \quad l_x = \frac{\sqrt{(E + \mu_{\sigma1})^2 - \Delta_{\eta\sigma1}^2} \cos\alpha_1}{\hbar v_F} ,$$

$$m_x = \frac{\sqrt{E^2 - \Delta_{\eta\sigma}^2} \cos\beta}{\hbar v_F} , \quad n_x = \frac{\sqrt{(E + \mu_{\sigma2})^2 - \Delta_{\eta\sigma2}^2} \cos\alpha_2}{\hbar v_F} , \tag{5.6}$$

where θ is the incident angle of electrons at the NM1/FM1 junction, α_1 is the incident angle at FM1/NM2 junction, β is the incident angle at NM2/FM2 junction, and α_2 is the incident angle at FM2/NM3 junction. These incident angles can be calculated via the conservation component in the y-direction as given by

$$k_{//} = \frac{\sqrt{E^2 - \Delta_{SO}^2}\,\sin\theta}{\hbar v_F} = \frac{\sqrt{(E + \mu_{\sigma 1})^2 - \Delta_{\eta\sigma 1}^2}\,\sin\alpha_1}{\hbar v_F}$$

$$= \frac{\sqrt{E^2 - \Delta_{\eta\sigma}^2}\,\sin\beta}{\hbar v_F} = \frac{\sqrt{(E + \mu_{\sigma 2})^2 - \Delta_{\eta\sigma 2}^2}\,\sin\alpha_2}{\hbar v_F} . \tag{5.7}$$

Therefore, the coefficients $r_{\eta\sigma}$, $a_{\eta\sigma}$, $b_{\eta\sigma}$, $g_{\eta\sigma}$, $f_{\eta\sigma}$, $p_{\eta\sigma}$, $q_{\eta\sigma}$, $t_{\eta\sigma}$ can be calculated by using the following boundary conditions.

$$\Psi_{NM1}(0) = \Psi_{FM1}(0), \quad \Psi_{FM1}(d) = \Psi_{NM2}(d),$$

$$\Psi_{NM2}(d+L) = \Psi_{FM2}(d+L), \quad \Psi_{FM2}(2d+L) = \Psi_{NM3}(2d+L), \tag{5.8}$$

where $r_{\eta\sigma}$ and $t_{\eta\sigma}$ represent reflection and transmission coefficients, respectively. Using the wave functions in Equation (5.4) and the boundary conditions in Equation (5.8), we can construct a matrix equation as follows:

$$
\begin{bmatrix}
1 & -1 & -1 & 0 & 0 & 0 & 0 & 0 \\
-Ae^{i\eta\theta} & -Be^{-i\eta\alpha_1} & Be^{i\eta\alpha_1} & 0 & 0 & 0 & 0 & 0 \\
0 & e^{il_xd} & e^{-il_xd} & -e^{im_xd} & -e^{-im_xd} & 0 & 0 & 0 \\
0 & Be^{-i\eta\alpha}e^{il_xd} & -Be^{i\eta\alpha_1}e^{-il_xd} & -Me^{-i\eta\beta}e^{im_xd} & Me^{i\eta\beta}e^{-im_xd} & 0 & 0 & 0 \\
0 & 0 & 0 & e^{im_x(d+L)} & e^{-im_x(d+L)} & -e^{in_x(d+L)} & -e^{-in_x(d+L)} & 0 \\
0 & 0 & 0 & Me^{-i\eta\beta}e^{im_x(d+L)} & -Me^{i\eta\beta}e^{-im_x(d+L)} & -Ne^{-i\eta\gamma}e^{in_x(d+L)} & Ne^{i\eta\gamma}e^{-in_x(d+L)} & 0 \\
0 & 0 & 0 & 0 & 0 & e^{in_x(2d+L)} & e^{-in_x(2d+L)} & -e^{ik_x(2d+L)} \\
0 & 0 & 0 & 0 & 0 & Ne^{-i\eta\alpha_2}e^{in_x(2d+L)} & -Ne^{i\eta\alpha_2}e^{-in_x(2d+L)} & -Ae^{-i\eta\theta}e^{ik_x(2d+L)}
\end{bmatrix}
\begin{bmatrix} r \\ a \\ b \\ g \\ f \\ p \\ q \\ t \end{bmatrix}
=
\begin{bmatrix} -1 \\ -Ae^{-i\eta\theta} \\ 0 \\ 0 \\ 0 \\ 0 \\ 0 \\ 0 \end{bmatrix}
$$

By using Cramer's rule and Mathematica tool, we can calculate the spin-valley conductance at the temperature of zero Kelvin in ballistic regime as explained in Chapter 4. In addition to spin polarization (SP) and valley polarization (VP) as defined in Equation (4.12), we also look at tunneling magnetoresistance (TMR) which can be defined as

$$TMR(\%) = \frac{G_P - G_{AP}}{G_P} \times 100, \tag{5.9}$$

where G_P and G_{AP} are respectively the total conductance in parallel (P) and anti-parallel (AP) junctions, when the total conductance can be expressed as $G_T = G_{k\uparrow} + G_{k\downarrow} + G_{k'\uparrow} + G_{k'\downarrow}$.

5.4 Results and Discussion

The analysis results are shown and discussed in this section. The dimension of the device structure is $d = 25$ nm, $L = 25$ nm, electrons excited energy is $E = 4$ meV, and chemical potential is $\mu = 2.5$ meV throughout this numerical analysis. The reason that we select the excited energy to be $E = 4$ meV is explained in Chapter 4.

In this chapter, we focus on the spin polarization, valley polarization, and tunnel magnetoresistance. Therefore, we utilize exchange field configuration No. 2 in Chapter 4 as the parallel junction (P) and a new anti-parallel junction (AP) to see the impact of light irradiation. The parallel and anti-parallel junctions are illustrated in Figure 5-3.

Spin-valley polarization is investigated as shown in Figure 5-4 which illustrates normalized conductance in P junction. Figure 5-4(a) is the result when there is no light irradiation, in which it depicts complete spin-valley polarization. This characteristic of perfect spin-valley polarization is useful for applications in spin-valley filtering devices. Figure 5-4(b) shows the junction under the same condition except that there is irradiation of 2000 THz light. The numerical analysis results indicate that the perfect spin-valley polarization is affected when electric field is nonzero. When there is no electric field, both Figure 5-4(a) and (b) show pure spin polarization. Although spin-valley polarization can still be noticed, meaningful applications from this results might be difficult considering the broad characteristics of $G_{k\uparrow}$ and $G_{k\uparrow}$.
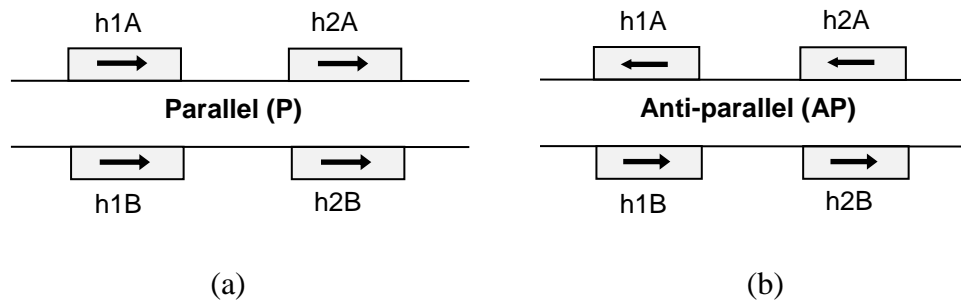

Figure 5-3: Configurations of magnetic exchange fields, where $\rightarrow$ represents h, and $\leftarrow$ represents $-h$. (a) Parallel junction, (b) Anti-parallel junction.
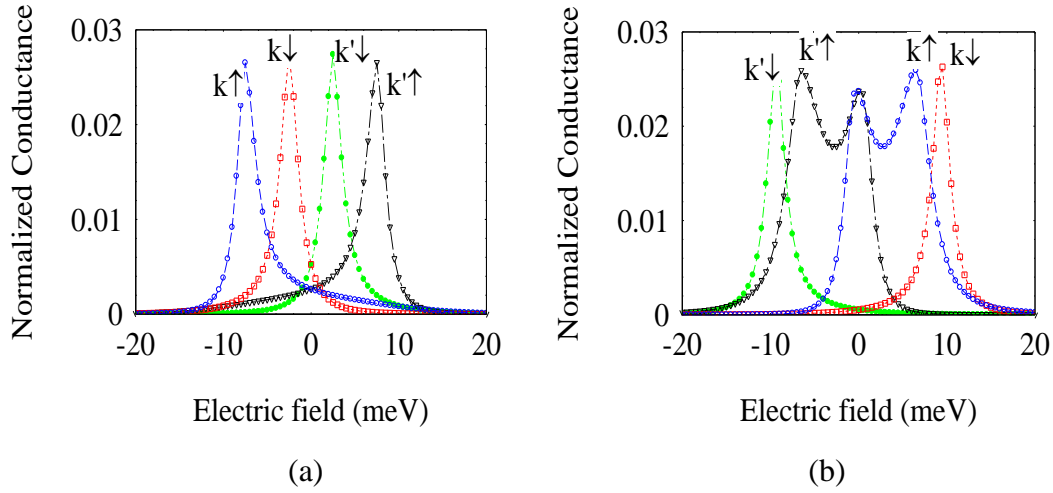
Figure 5-4: Conductance in P junction when (a) there is no light irradiation, (b) there is irradiation of 2000 THz light.

Spin polarization (SP) with increasing external electric field E_z at the ferromagnetic gates when there is no light irradiation on P junction and AP junction is shown in Figure 5-5(a) and Figure 5-5(b), respectively. The comparison of the two figures illustrates the impact of exchange field configuration on the spin polarization. Figure 5-5(a) shows full switching from $+100\%$ to -100% at near 0 meV in AP junction, while Figure 5-5(b) shows relatively modest spin polarization in P junction.

In the case of light irradiation with frequency of 1000 THz, 1500 THz and 2000 THz, the spin polarization characteristics in P junction and AP junction are shown in Figure 5-5(c) and Figure 5-5(d), respectively. Comparisons of Figure 5-5(c) to Figure 5-5(a) and Figure 5-5(d) to Figure 5-5(b) clearly depict the effect of light irradiation in both exchange field configurations, where the light frequency also play significant role. The results show that the range of spin polarization is significantly enhanced in P junction as seen in Figure 5-5(c). Particularly when the light frequency of 1000 THz is applied, the spin polarization switches from -100% to $+100\%$ in the negative electric field region, and from $+100\%$ to -100% in the positive electric field region. On the other hand, Figure 5-5(d) shows oscillation of spin polarization when the electric field is increased. Particularly in the case that the applied light frequency is 2000 THz, the oscillation is clear.
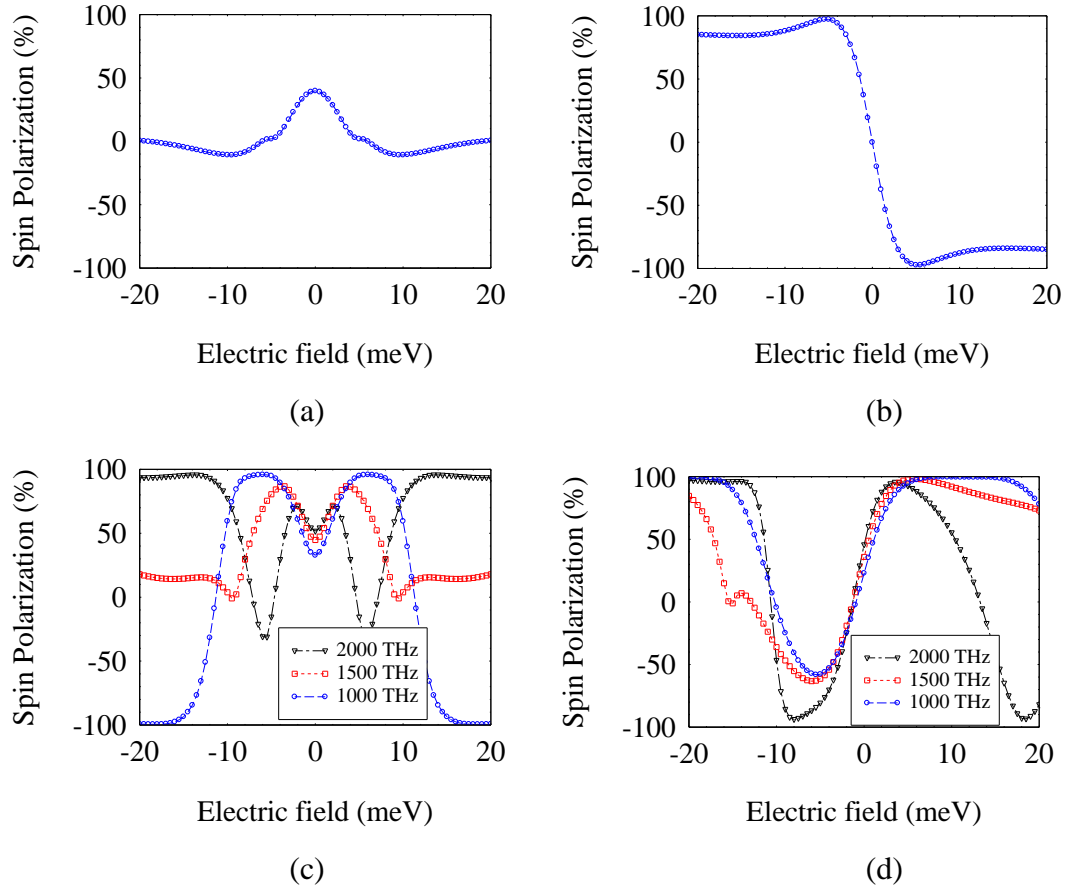
Figure 5-5: Spin polarization when there is no light irradiation in (a) P junction, (b) AP junction, and when there is light irradiation of 1000 THz, 1500 THz, and 2000 THz in (c) P junction, (d) AP junction.

Valley polarization (VP) characteristics are shown in Figure 5-6. Similarly to the case of spin polarization, Figure 5-6(a) and (b) are the cases of no light irradiation to P junction and AP junction, where the exchange field configuration affects the characteristics of valley polarization. However, in the opposite to spin polarization in Figure 5-5 where the full switching occurred in AP junction, the valley polarization shows full switching from $+100\%$ to -100% near the electric field of 0 meV in P junction as shown in Figure 5-6(a). Figure 5-6(c) and (d) is valley polarization when the light with frequency of 1000 THz, 1500 THz and 2000 THz is irradiated to P junction and AP junction, respectively. It is interesting that both junctions show very similar characteristics. Neither exchange field nor light frequency has significant impact on the valley polarization characteristics, which show sharp full switching from -100% to $+100\%$, especially in P junction. The results depict potentials for applications in valleytronics.
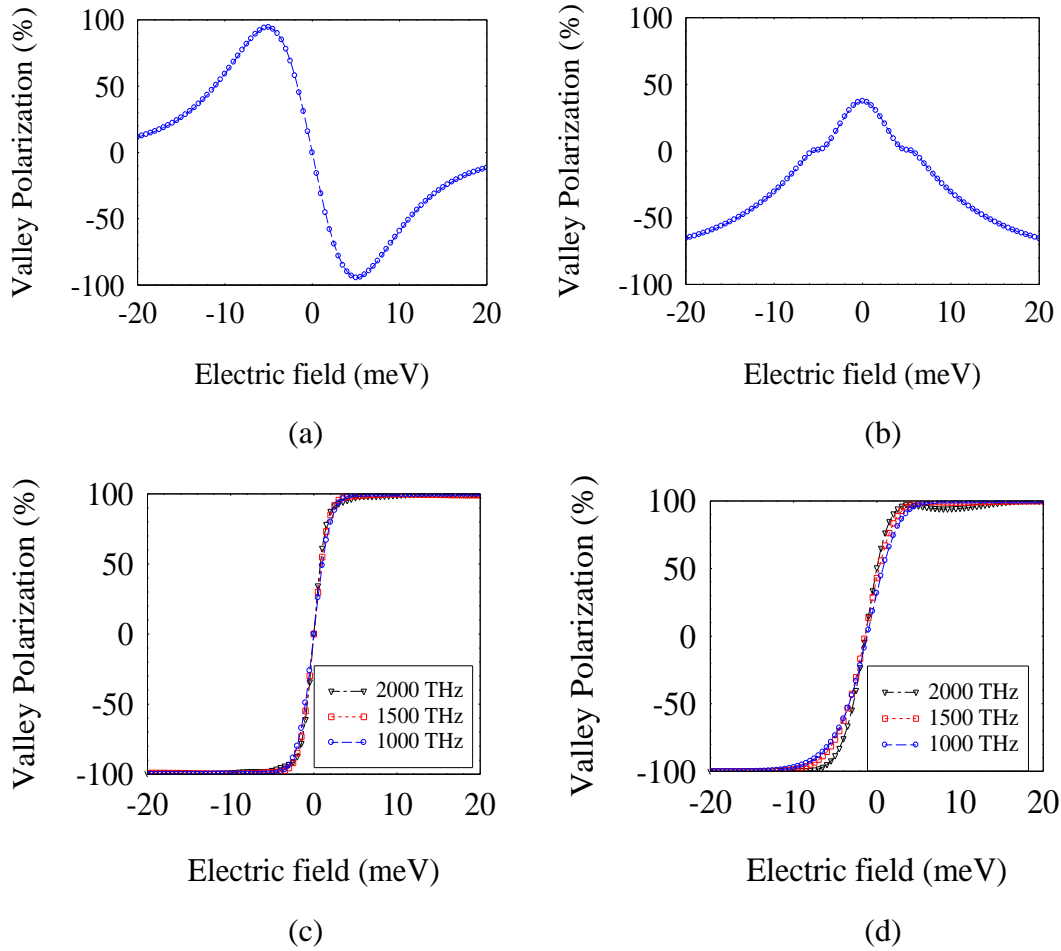
Figure 5-6: Valley polarization when there is no light irradiation in (a) P junction, (b) AP junction, and when there is light irradiation of 1000 THz, 1500 THz, and 2000 THz in (c) P junction, (d) AP junction.

We also investigate the impact of photo irradiation on the tunnel magnetoresistance (TMR) characteristics as shown in Figure 5-7(b) where light with frequency of 1000 THz, 1500 THz and 2000 THz are irradiated. Comparing it to Figure 5-7(a) where there is no light irradiation, it shows that the amplitudes of TMR increase significantly with photo irradiation. The changes of electron transport characteristics as seen in SP, VP, and TMR from Figure 5-3 to Figure 5-7 are considered to be the results of photon dressing effect due to circularly polarized photo irradiation. With the photon dressing effect, the band structure and change electronic properties of the materials might be modified as explained in Section 5.2.
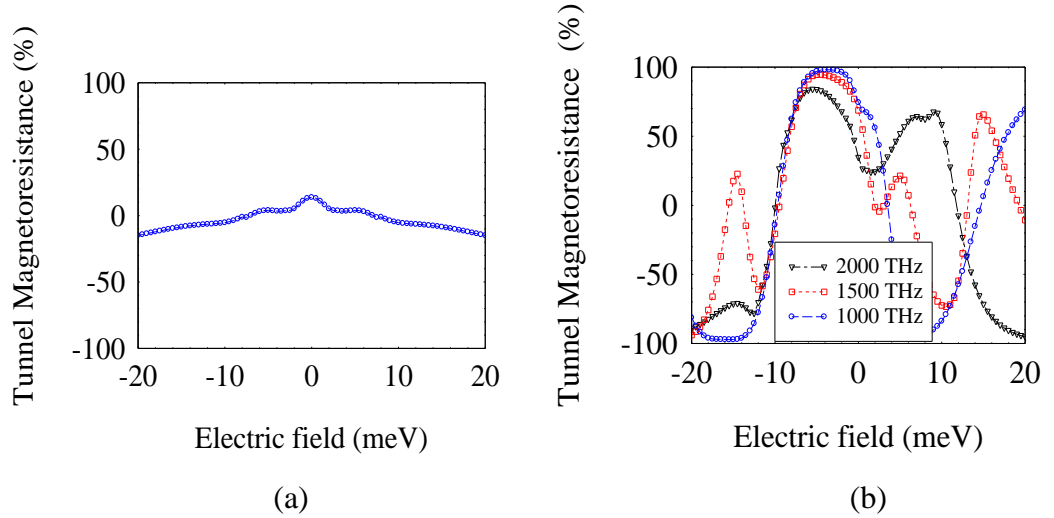
Figure 5-7: Tunnel magnetoresistance when there is (a) no light, (b) light irradiation.

5.5 Conclusions

In this chapter we have studied the photo effects on the spin-valley transport in our proposed dual ferromagnetic gate silicene-based device structure. It is found that all components of the polarized spin-valley currents ($k\uparrow, k\downarrow, k'\uparrow, k'\downarrow$) in both P and AP junctions are affected by the light irradiation. This might be due to photon dressing effect, which is modification of the band structure and change electronic properties from the application of light on silicene. We found that the range of spin polarization (SP) is enhanced in P junction, and shows oscillation of SP in AP junction. Valley polarization (VP) is affected in different way from spin polarization. Both P junction and AP junction show similar characteristics with photo irradiation, and either exchange field configuration or light frequency has no significant impact on valley polarization. It was also discovered that photo irradiation has strong impact on tunnel magnetoresistances (TMR) causing the amplitude to increase significantly. We further investigate the light irradiation effect in Chapter 6 towards device applications.

Chapter 6

Spin-Valleytronic Photo-Sensing Device

In Chapter 5 we have investigated the electronic transport properties of dual ferromagnetic-gated silicene-based device structure when circularly polarized photo irradiation is applied to the NM2 region between the ferromagnetic gates under the influence of electric fields, chemical potentials, and magnetic exchange fields. The objective is to understand basic characteristics of proposed device structure under light irradiation. In this chapter, we further our investigation by adding more exchange field configurations with the objective to find the optimized conditions of the proposed structure for applications in spin-valleytronic photo-sensing devices. We particularly look at the conductance, in addition to spin polarization, valley polarization, and tunnel magnetoresistance as investigated in Chapter 5.

6.1 Device Models

The device structure used in our investigation in this chapter is almost the same as in Chapter 5 including the device parameters d and L as illustrated in Figure 6-1. There are two differences in the conditions and device structure used in this chapter and that in Chapter 5. The first difference is the existence of one more anti-parallel junction (AP) added into magnetic exchange field configurations as shown in Figure 6-2. The Figure 6-2(a) shows parallel junction, Figure 6-2(b) shows anti-parallel junction No.1 (AP-1) which is the anti-parallel junction (AP) in Chapter 5, and Figure 6-2(c) illustrates anti-parallel junction No.2 (AP-2) which is a newly added exchange field configuration in this chapter. The objective of this additional exchange field configuration is to identify the optimized condition for

filtering effect for specific spin-valley component as seen for $k \uparrow$ current component in Figure 5-5(b). Another difference is additional electric field to NM2 region as depicted in Figure 6-1, where the electric field on ferromagnetic gates is labeled as E_{z1} and the electric field on NM2 region is labeled as E_{z2}.
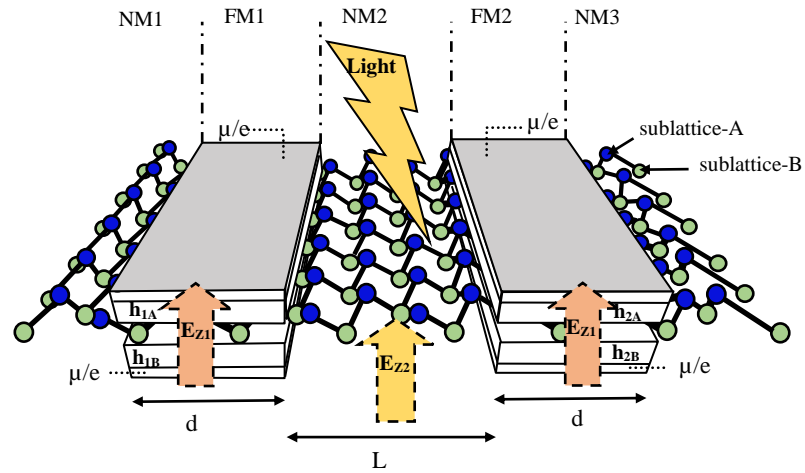

Figure 6-1: Schematic model of proposed structure NM1/FM1/NM2/FM2/NM3 with light irradiation and additional electric field E_{z2} on NM2 region.
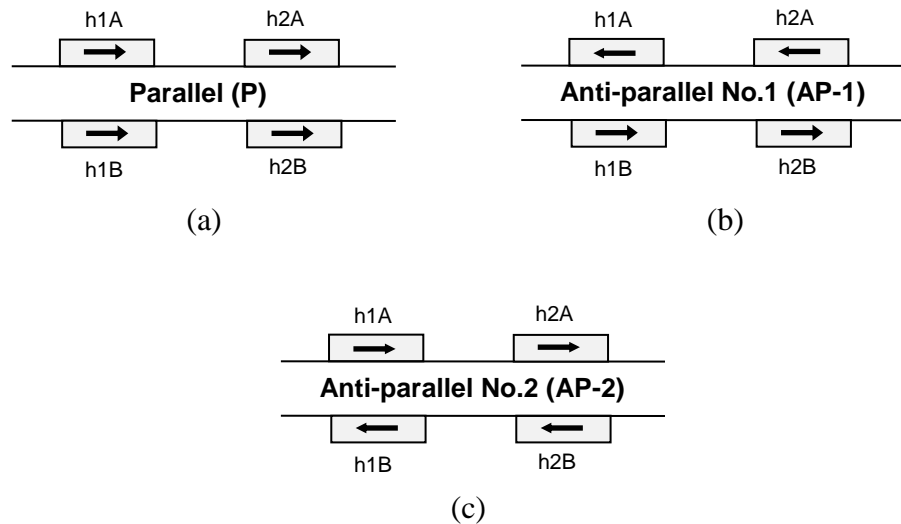

Figure 6-2: Configurations of magnetic exchange fields, where $\rightarrow$ represents h, and $\leftarrow$ represents ^{-}h. (a) Parallel junction, (b) anti-parallel junction No.1 (AP-1), (c) anti-parallel junction No.2 (AP-2).

Tight-binding model is used to define low-energy effective Hamiltonians in the same manner as in Chapter 5. The Hamiltonians for the ferromagnetic regions FM1 and FM2 are defined as

$$H_{\eta\sigma} = v_F(p_x\tau_x - \eta p_y\tau_y) - \Delta_{\eta\sigma1}\tau_z - \mu_{\sigma1}$$

$$H_{\eta\sigma} = v_F(p_x\tau_x - \eta p_y\tau_y) - \Delta_{\eta\sigma2}\tau_z - \mu_{\sigma2}, \tag{6.1}$$

respectively. The notations η and σ respectively represent valley and spin. Spin-valley dependent energy gaps are $\Delta_{\eta\sigma1} = \eta\sigma\Delta_{SO} - \Delta_{E1} + \sigma\Delta_{M1}$ and $\Delta_{\eta\sigma2} = \eta\sigma\Delta_{SO} - \Delta_{E1} + \sigma\Delta_{M2}$, where electric field-induced energy gap is $\Delta_{E1} = eDE_{z1}$, and the exchange field-induced energy gaps are $\Delta_{M1} = \dfrac{(h_{1A} - h_{1B})}{2}$, $\Delta_{M2} = \dfrac{(h_{2A} - h_{2B})}{2}$. The spin-dependent chemical potentials could be defined with $\mu_{\sigma1} = \mu + \sigma u_{M1}$ and $\mu_{\sigma2} = \mu + \sigma u_{M2}$, where $u_{M1} = \dfrac{h_{1A} + h_{1B}}{2}$ and $u_{M2} = \dfrac{h_{2A} + h_{2B}}{2}$.

The Hamiltonian in normal region NM2 with photo irradiation can be described as

$$H_{\eta\sigma} = v_F(p_x\tau_x - \eta p_y\tau_y) - \Delta_{\eta\sigma}\tau_z, \tag{6.2}$$

where Spin-valley dependent energy gap is $\Delta_{\eta\sigma} = \eta\sigma\Delta_{SO} - \Delta_{E2} + \eta\lambda_\Omega$. The notations $\Delta_{E2} = eDE_{z2}$ and $\lambda_\Omega = (e\Lambda V_F)^2/\hbar\Omega$, respectively. We use $\Lambda = eA_0a/\hbar$ which is a dimensionless number to characterize the light intensity with e represents the elementary charge, A_0 represents the magnitude of light wave, and a represents the lattice constant of silicene. The value of Λ is generally less than 1 for the intensity from light sources in the frequency range of our interest.

In the normal regions NM1 and NM3, where there is neither photo irradiation nor external electric field, the spin-valley dependent energy gap is $\Delta_{\eta\sigma3} = \eta\sigma\Delta_{SO}$. Therefore, the Hamiltonian in these two regions could be defined as

$$H_{\eta\sigma} = v_F(p_x\tau_x - \eta p_y\tau_y) - \eta\sigma\Delta_{so}\tau_z. \tag{6.3}$$

Solving the Hamiltonians, when the spin-valley currents flow in the x-direction, yields the wave function in each region as follows:

$$\Psi_{NM1} = \left[\begin{pmatrix} 1 \\ A_{\eta\sigma}e^{-i\eta\theta} \end{pmatrix} e^{ik_x x} + r_{\eta\sigma} \begin{pmatrix} 1 \\ -A_{\eta\sigma}e^{i\eta\theta} \end{pmatrix} e^{-ik_x x} \right] e^{ik_{//}y}$$

$$\Psi_{FM1} = \left[a_{\eta\sigma} \begin{pmatrix} 1 \\ B_{\eta\sigma}e^{-i\eta\alpha_1} \end{pmatrix} e^{il_x x} + b_{\eta\sigma} \begin{pmatrix} 1 \\ -B_{\eta\sigma}e^{i\eta\alpha_1} \end{pmatrix} e^{-il_x x} \right] e^{ik_{//}y}$$

$$\Psi_{NM2} = \left[g_{\eta\sigma} \begin{pmatrix} 1 \\ M_{\eta\sigma}e^{-i\eta\beta} \end{pmatrix} e^{im_x x} + f_{\eta\sigma} \begin{pmatrix} 1 \\ -M_{\eta\sigma}e^{i\eta\beta} \end{pmatrix} e^{-im_x x} \right] e^{ik_{//}y}$$

$$\Psi_{FM2} = \left[p_{\eta\sigma} \begin{pmatrix} 1 \\ N_{\eta\sigma}e^{-i\eta\alpha_2} \end{pmatrix} e^{in_x x} + q_{\eta\sigma} \begin{pmatrix} 1 \\ -N_{\eta\sigma}e^{i\eta\alpha_2} \end{pmatrix} e^{-in_x x} \right] e^{ik_{//}y}$$

$$\Psi_{NM3} = \left[t_{\eta\sigma} \begin{pmatrix} 1 \\ A_{\eta\sigma}e^{-i\eta\theta} \end{pmatrix} e^{ik_x x} \right] e^{ik_{//}y} , \tag{6.4}$$

where parameters

$$A_{\eta\sigma} = \frac{E + \eta\sigma\Delta_{SO}}{\sqrt{E^2 - \Delta_{SO}^2}}, \quad B_{\eta\sigma} = \frac{E + \mu_{\sigma1} + \Delta_{\eta\sigma1}}{\sqrt{(E + \mu_{\sigma1})^2 - \Delta_{\eta\sigma1}^2}}$$

$$M_{\eta\sigma} = \frac{E + \Delta_{\eta\sigma}}{\sqrt{E^2 - \Delta_{\eta\sigma}^2}}, \text{ and } N_{\eta\sigma} = \frac{E + \mu_{\sigma2} + \Delta_{\eta\sigma2}}{\sqrt{(E + \mu_{\sigma2})^2 - \Delta_{\eta\sigma2}^2}}. \tag{6.5}$$

Then the wave vectors in x-direction of electron in NMs and FMs regions are described by

$$k_x = \frac{\sqrt{E^2 - \Delta_{SO}^2}\cos\theta}{\hbar v_F}, \quad l_x = \frac{\sqrt{(E + \mu_{\sigma1})^2 - \Delta_{\eta\sigma1}^2}\cos\alpha_1}{\hbar v_F},$$

$$m_x = \frac{\sqrt{E^2 - \Delta_{\eta\sigma}^2}\cos\beta}{\hbar v_F}, \quad n_x = \frac{\sqrt{(E + \mu_{\sigma2})^2 - \Delta_{\eta\sigma2}^2}\cos\alpha_2}{\hbar v_F}, \tag{6.6}$$

where θ is the incident angle of electrons at the NM1/FM1 junction, α_1 is the incident angle at FM1/NM2 junction, β is the incident angle at NM2/FM2 junction, and α_2 is the incident angle at FM2/NM3 junction.

These incident angles can be calculated via the conservation component in the y-direction as given by

$$k_{//} = \frac{\sqrt{E^2 - \Delta_{SO}^2}\,\sin\theta}{\hbar v_F} = \frac{\sqrt{(E + \mu_{\sigma 1})^2 - \Delta_{\eta\sigma 1}^2}\,\sin\alpha_1}{\hbar v_F}$$

$$= \frac{\sqrt{E^2 - \Delta_{\eta\sigma}^2}\,\sin\beta}{\hbar v_F} = \frac{\sqrt{(E + \mu_{\sigma 2})^2 - \Delta_{\eta\sigma 2}^2}\,\sin\alpha_2}{\hbar v_F}. \tag{6.7}$$

Therefore, the coefficients $r_{\eta\sigma}$, $a_{\eta\sigma}$, $b_{\eta\sigma}$, $g_{\eta\sigma}$, $f_{\eta\sigma}$, $p_{\eta\sigma}$, $q_{\eta\sigma}$, $t_{\eta\sigma}$ can be calculated by using the following boundary conditions.

$$\Psi_{NM1}(0) = \Psi_{FM1}(0)\,, \quad \Psi_{FM1}(d) = \Psi_{NM2}(d)\,,$$

$$\Psi_{NM2}(d+L) = \Psi_{FM2}(d+L)\,, \quad \Psi_{FM2}(2d+L) = \Psi_{NM3}(2d+L)\,, \tag{6.8}$$

where $r_{\eta\sigma}$ and $t_{\eta\sigma}$ represent reflection and transmission coefficients, respectively. Using the wave functions in Equation (6.4) and the boundary conditions in Equation (6.8), we can construct a matrix equation as follows:

$$\begin{bmatrix} 1 & -1 & -1 & 0 & 0 & 0 & 0 & 0 \\ -Ae^{i\eta\theta} & -Be^{-i\eta\alpha_1} & Be^{i\eta\alpha_1} & 0 & 0 & 0 & 0 & 0 \\ 0 & e^{il_xd} & e^{-il_xd} & -e^{im_xd} & -e^{-im_xd} & 0 & 0 & 0 \\ 0 & Be^{-i\eta\alpha}e^{il_xd} & -Be^{i\eta\alpha_1}e^{-il_xd} & -Me^{-i\eta\beta}e^{im_xd} & Me^{i\eta\beta}e^{-im_xd} & 0 & 0 & 0 \\ 0 & 0 & 0 & e^{im_x(d+L)} & e^{-im_x(d+L)} & -e^{in_x(d+L)} & -e^{-in_x(d+L)} & 0 \\ 0 & 0 & 0 & Me^{-i\eta\beta}e^{im_x(d+L)} & -Me^{i\eta\beta}e^{-im_x(d+L)} & -Ne^{-i\eta\gamma}e^{in_x(d+L)} & Ne^{i\eta\gamma}e^{-in_x(d+L)} & 0 \\ 0 & 0 & 0 & 0 & 0 & e^{in_x(2d+L)} & e^{-in_x(2d+L)} & -e^{ik_x(2d+L)} \\ 0 & 0 & 0 & 0 & 0 & Ne^{-i\eta\alpha_2}e^{in_x(2d+L)} & -Ne^{i\eta\alpha_2}e^{-in_x(2d+L)} & -Ae^{-i\eta\theta}e^{ik_x(2d+L)} \end{bmatrix} \begin{bmatrix} r \\ a \\ b \\ g \\ f \\ p \\ q \\ t \end{bmatrix} = \begin{bmatrix} -1 \\ -Ae^{-i\eta\theta} \\ 0 \\ 0 \\ 0 \\ 0 \\ 0 \\ 0 \end{bmatrix}$$

By using Cramer's rule and Mathematica tool, we can calculate the spin-valley conductance at the temperature of zero Kelvin in ballistic regime as already explained in Chapter 4.

6.2 Results and discussion

The normalized conductance when the frequency of circularly polarized light increases and there is no electric field ($E_{z1} = E_{z2} = 0$ meV) is shown in Figure 6-3. The Figure 6-3(a) depicts pure spin polarization in parallel junction which coincides with the result shown in the Figure 4-4(b) in Chapter 4 and Figure 5-4(a), (b) in Chapter 5 at $E_z = 0$ meV, where the exchange field configuration is the same. It is interesting to see that the conductance shows pure spin-valley polarization where $G_{k\uparrow} \neq G_{k\downarrow} \neq G_{k'\uparrow} \neq G_{k'\downarrow}$ under increasing light frequency in anti-parallel junctions as illustrated in Figure 6-3(b) and (c).
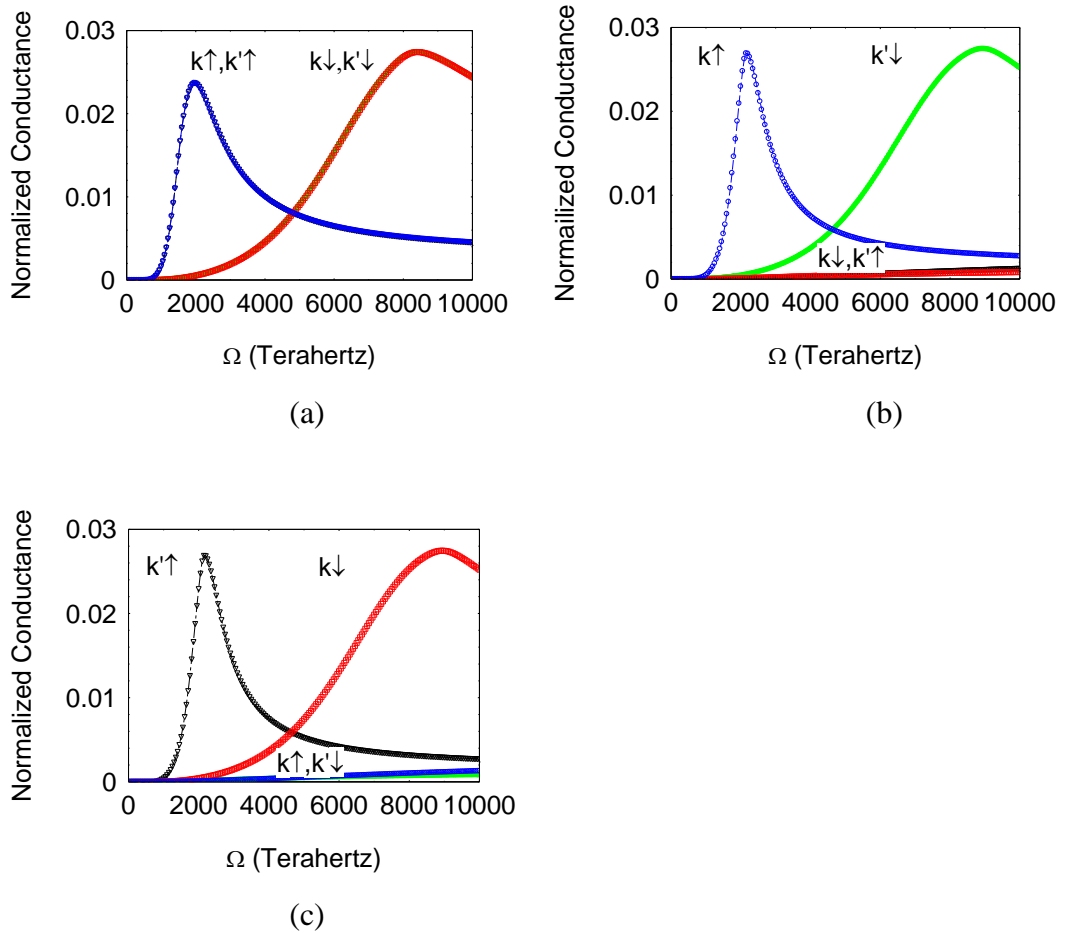

(a)

(b)

(c)

Figure 6-3: Normalized conductance when the light frequency increases with no electric fields ($E_{z1} = E_{z2} = 0$ meV) and $\mu = 2.5$ meV in (a) P junction, (b) AP-1 junction, and (c) AP-2 junction.

When external electric field E_{Z1} is applied to ferromagnetic barriers (FM1 and FM2) and another external electric field E_{Z2} is applied to normal region NM2 along with circularly polarized light, the device structure exhibits interesting characteristics as shown in Figure 6-4. When $E_{Z1} = E_{Z2} = +4$ meV, sharp $k \uparrow$ peak appears near the frequency of 2,000 terahertz in AP-1 configuration, and sharp $k \downarrow$ peak appears near the similar frequency in AP-2 configuration as indicated in Figure 6-4(a) and Figure 6-4(b), respectively. In the similar manner, when $E_{Z1} = E_{Z2} = -4$ meV, $k'\downarrow$ and $k'\uparrow$ peaks appear near 2000 terahertz in AP-1 and AP-2 configurations as depicted in Figure 6-4(c) and Figure 6-4(d), respectively.
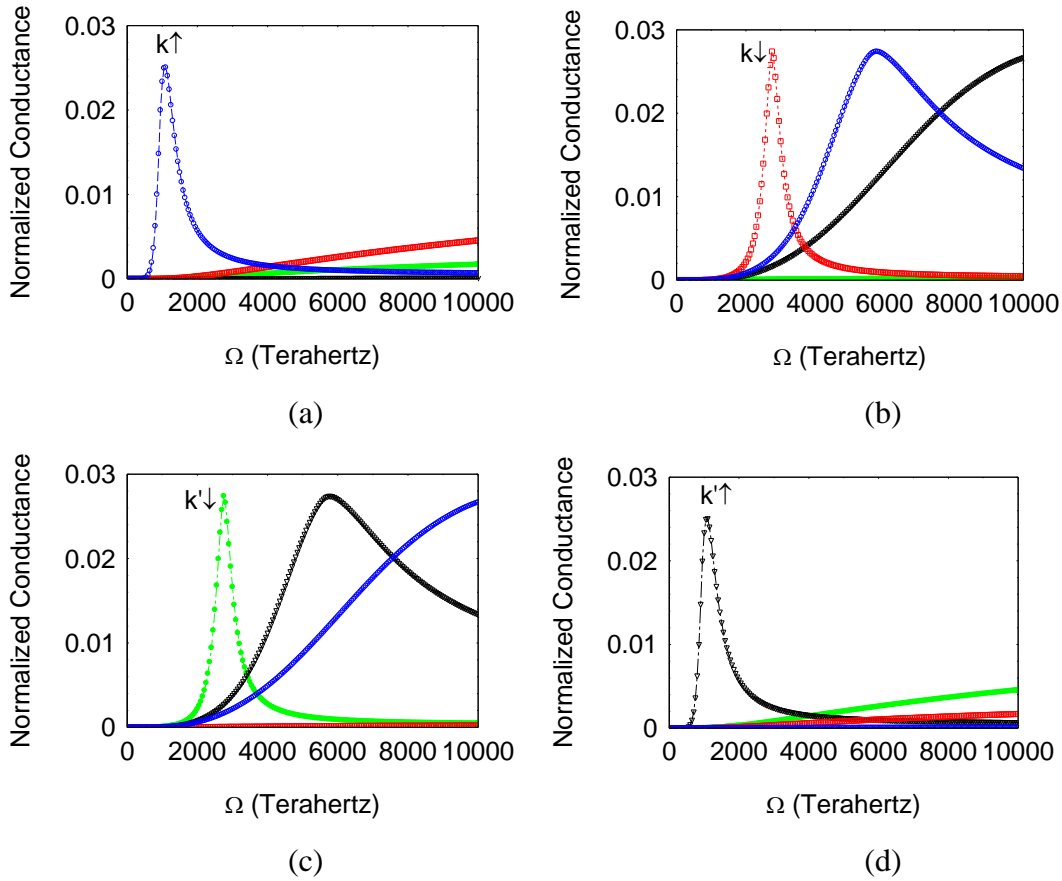

(a)

(b)

(c)

(d)

Figure 6-4: Normalized conductance when the light frequency increases in anti-parallel junctions where $\mu = 2.5$ meV, when $E_{Z1} = E_{Z2} = +4$ meV in (a) AP-1 junction, (b) AP-2 junction, and when $E_{Z1} = E_{Z2} = -4$ meV in (c) AP-1 junction (d) AP-2 junction.

The comparison of Figure 6-3(b) and Figure 6-4(a) illustrates the suppression of $k'\downarrow$ component by positive electric field, while the comparison of Figure 6-3(c) and Figure 6-4(d) illustrates the suppression of $k\downarrow$ component by negative electric field. This is considered to be the results of filtering effects from the ferromagnetic barriers with the application of external electric field. In other words, we can select the spin-valley component to be filtered by properly manipulating the direction of electric fields E_{Z1} and E_{Z2} as well as the exchange fields configuration at the barriers. It indicates that our proposed dual-barrier silicene-based structure might behave as a filter for specific spin-valley polarization.

It was discovered that tunneling magnetoresistance (TMR) is also controllable by electric fields and chemical potential under photo irradiation as illustrated in Figure 6-5. The Equation (5.9) in Chapter 5 is used to define TMR, where the AP-1 configuration is used to represent G_{AP}. Figure 6-5(a) exhibits the dependency of TMR on electric fields where $E_Z = E_{Z1} = E_{Z2}$ and the irradiated light frequency. It shows that the minimum value of TMR becomes lower and the minimum point shifts toward lower light frequency, as the electric fields E_{Z1} and E_{Z2} increase. Particularly when the electric fields are 6 meV, the minimum of TMR is lower than $-2,200\%$ which is a significant increase from -73% when the electric fields are 4 meV. This huge TMR at 6 meV indicates giant magnetoresistance (GMR) due to the low total resistance in P junction (G_P) but high total resistance in AP junction (G_{AP}).

Figure 6-5(b) also shows similar correlation of TMR with gate-induced chemical potential μ, where higher chemical potential results in lower minimum point of TMR at lower frequency. It is interesting to see the similar result to Figure 6-5(a) that GMR also shows up here. The minimum value of TMR increases significantly from -19% when $\mu = 5.0$ meV to around -570% when $\mu = 7.5$ meV. The TMR characteristics in Figure 6-5 indicate that the external electric fields and chemical potential may have a significant impact on electron scattering at a certain light frequency, when the strength of electric fields and chemical potential reaches a certain level.
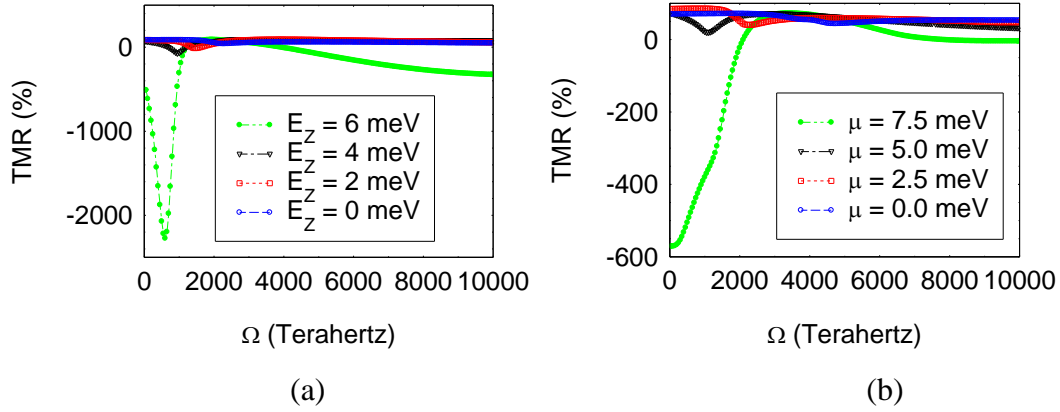
Figure 6-5: Tunneling magnetoresistnace when the light frequency increases in AP-1 junctions where $E_Z = E_{Z1} = E_{Z2}$ under the conditions that (a) μ = 2.5 meV and E_Z is varied from 0 to 6 meV, (b) E_Z = 0 meV and μ is varied from 0 to 7.5 meV.

From Figure 6-3, we see that Figure 6-3(a) exhibits pure spin polarization in P junction, while Figure 6-3(b) exhibits pure spin-valley polarization in AP-1 junction when there is no electric fields. Therefore, we examine the spin polarization (SP) in P junction and valley polarization (VP) in AP-1 junction as a function of light frequency with varying chemical potential μ when there is no electric field. The spin polarization and valley polarization characteristics are shown in Figure 6-6(a) and Figure 6-6(b), respectively. This control of SP and VP characteristics with chemical potential is mainly due to the quantum interference of electrons in ferromagnetic gates. Another interesting result is that both SP and VP exhibit almost exactly the same characteristics in μ = 0 meV and μ = 2.5 meV as depicted in Figure 6-6(a) and Figure 6-6(b), respectively. However, when the chemical potential μ increases to 5.0 meV and 7.5 meV, SP shows less dependency on light frequency, while VP stays almost unchanged.

We have discussed the possibility to apply this device structure as a filter for specific spin-valley polarization in Figure 6-4. Particularly, Figure 6-4(a) indicates the condition for k↑ filtering, where positive electric fields ($E_{Z1} = E_{Z2} = +4$ meV) and chemical potential μ = 2.5 meV are applied to AP-1 junction. Therefore, we further the investigation to see the impact of the distance L between ferromagnetic gates on the spin-valley polarization in AP-1 junction with the objective to have better understanding for future applications.
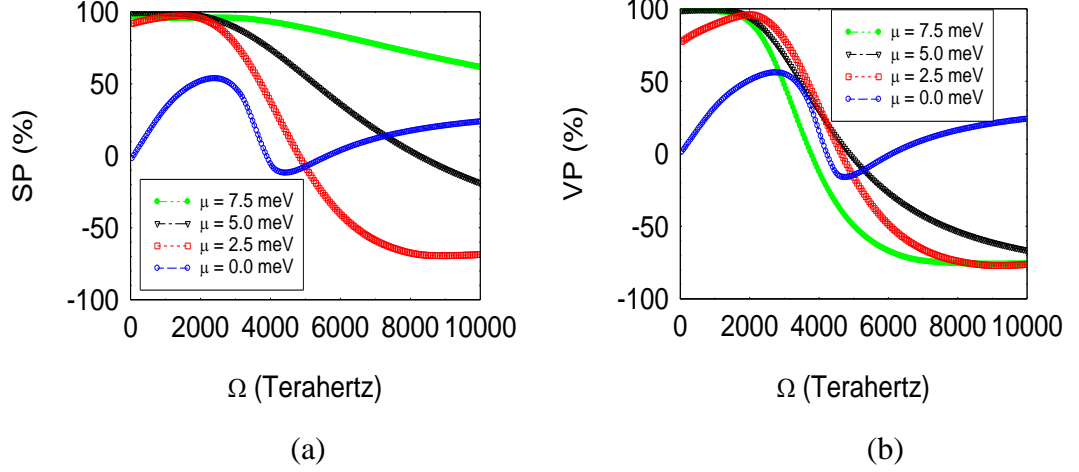
Figure 6-6: When the light frequency increases without electric field ($E_{z1} = E_{z2} = 0$ meV) and μ is varied from 0 to 7.5 meV, (a) spin polarization in P junctions, and (b) valley polarization in AP-1 junctions.

The Figure 6-7(a) shows $k\uparrow$ current characteristics under the same conditions as in Figure 6-4(a) with varied value of distance L. The shifting of $k\uparrow$ current peaks toward higher light frequency indicates that the filtering effect on $k\uparrow$ comes from resonance, where the smaller L causes resonance to occur at lower light frequency and vice versa.

Figure 6-7(b) shows each component of the spin-valley polarized current when distance $L = 50$ nm. Comparison of Figure 6-7(b) to Figure 6-4(a) where $L = 25$ nm shows that only $k\uparrow$ is affected by the change of L. That confirms our understanding that the distance L affects only filtered spin-valley current, while other spin-valley components are almost unchanged. In addition to the spin-valley polarized current, total conductance is also an important parameter from practical point of view.

Figure 6-7(c) shows the total conductance combining all spin-valley currents with varied distance L between the ferromagnetic gates FM1 and FM2. The total conductance characteristics have maximum point at a certain light frequency representing the possibility of applications in polarized-photon frequency filter. This is because total conductance is normally used in the real-world applications. Furthermore, the results indicate that the light frequency which yields the maximum conductance might be controlled by the distance between barriers.
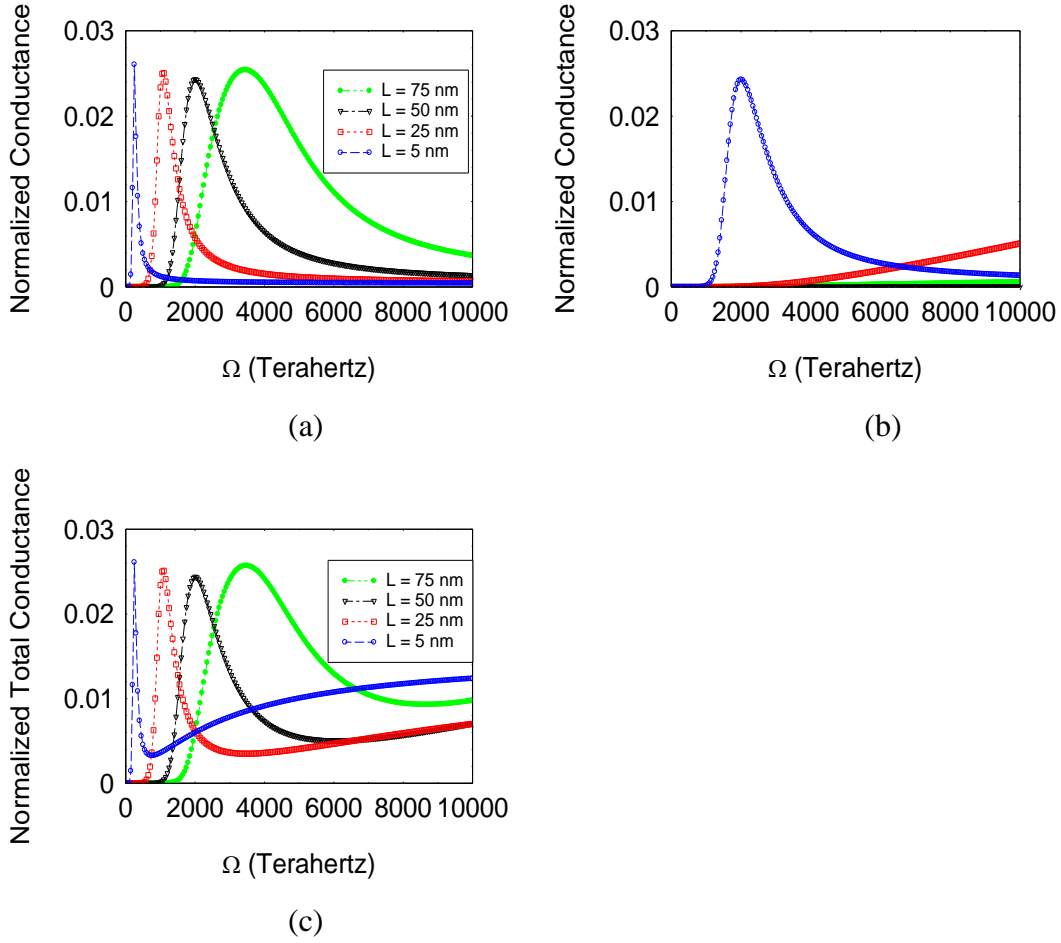
Figure 6-7: Effects of the distance *L* between ferromagnetic gates in AP-1 junction. (a) Conductance component k↑ current with varied *L*. (b) Conductance of each spin-valley component when *L* = 50nm. (c) Total conductance of all spin-valley components with varied *L*.

It is worth to add a discussion here about the internal interaction among magnetic exchange field components. From Chapter 4 to Chapter 6 we use multiple magnetic exchange field configurations, in which there are two components for each ferromagnetic gate totaling four components in the structure. Since the thickness of stable low-buckling silicene is estimated to be 0.46 Å, this extremely small distance may allow the interaction between magnetic fields from magnetic insulator h_{1A} and h_{1B} on FM1, and between magnetic fields from magnetic insulator h_{2A} and h_{2B} on FM2. However, the tight-binding model utilized in our study does not include this internal interaction for the simplicity of the model and analysis.

The validity and accuracy of the results from tight-binding model being used in our analysis is discussed here before we go to the conclusion in the next section. Although it is impossible to directly compare the theoretical results from this study with the results from experiments due to the technical challenges facing the realization of free-standing silicene, it is possible to make clear statement regarding the validity and accuracy of our work. First, tight-binding is a widely used fully-quantum-mechanical approach as introduced in more details in Section 3.2. One reason behind its popularity is its simplicity and efficiency [113-115]. The accuracy of this tight-binding approximation has increased over the time with improvement, such as the inclusion of total-energy calculations and density functional approach [116, 117]. In this dissertation we use the standard tight-binding model which expands the eigenstates of Hamiltonians. In term of the accuracy of tight-binding approximation for work in elemental 2D materials such as graphene and silicene, there have been results discussing this issue and showing the effectiveness of this method [104, 118, 119].

6.3 Conclusions

We have investigated the spin-valley transport in dual ferromagnetic-gate silicene-based junctions under circularly polarized light irradiation. When there is no electric field and the exchange energy configuration is parallel, the spin-valley conductance shows pure spin polarization similar to the case of no light irradiation. It is interesting to see that the device structure shows spin-valley filtering characteristics when electric fields E_{Z1} and E_{Z2} are applied to anti-parallel junctions. In this case, we can select specific spin-valley polarization to be filtered by providing appropriate conditions, such as the direction of electric fields and exchange field configuration.

We also discovered that by adjusting the distance L between two ferromagnetic gates, the light frequency for the appearance of spin-valley polarization peak can be controlled. Our investigation revealed a possibility to control tunneling magnetoresistance (TMR) with electric fields and gate-induced chemical potentials under the photo-irradiation regime. It is found that TMR

magnitude may change significantly at a specific light frequency when the strength of electric field or chemical potential reaches a certain level. The TMR can be categorized as GMR, when TMR is $-2,200\%$ at electric fields of 6 meV, and -570% at chemical potential of 7.5 meV. We also successfully demonstrate the control of SP and VP over the increasing light frequency by adjusting chemical potentials μ.

Chapter 7

Conclusions and Future Work

7.1 Summary of This Dissertation

In this dissertation, we have explained the motivation behind investigation of electronic transportation in silicene, and reviewed the research activities on this attractive material. There have been many studies on the effect of electric field, exchange field, and photo irradiation on silicene. However, none of them has investigated the effect on double-ferromagnetic barrier structure, which is the main scope of this dissertation. The work in this dissertation is theoretical approach using tight-binding model to obtain the effective Hamiltonian of the device structure. Then Mathematica, widely used symbolic computation software, was used to helping solving the equation to get conductance, which is used to analyze the spin-polarized, valley-polarized, and pseudospin-polarized currents as well as the tunnel magnetoresistance of the device.

In Chapter 4 we predict that the proposed device structure can be switched from a pure spin-polarizer to a pure valley-polarizer. It also demonstrates perfect control of spin-valley currents by adjusting the configuration of exchange fields. It is also found that specific exchange field configurations might destroy spin-valley filtering polarization and instead yield pure sublattice pseudospin polarization, where the polarized current flows solely in either sublattice-A or sublattice-B. This pseudospin polarized current can be achieved only in dual ferromagnetic-gated junctions, and is not achievable in single ferromagnetic-gated junctions.

In Chapter 5 and Chapter 6, we investigated the effect of circularly polarized light illumination on the same device structure under the influence of electric field and exchange field. The results show the possibility of spin-valley filtering which can be achieved at the off-resonant frequency region with

appropriate controls of electric fields and exchange fields. The analysis also suggests the possibility to control tunneling magnetoresistance (TMR) to become giant magnetoresistance (GMR) by adjusting electric fields or chemical potentials. With the research results presented in this dissertation, one potential application is photo-sensing devices using spin-polarized current and valley-polarized current. We expect this dissertation to make contributions to the further development in the field of spintronics, valleytronics, and pseudospintronics.

7.2 Future Work

Our proposed silicene-based double-ferromagnetic barrier structure shows the potential to control spin-polarized current, valley-polarized current, pseudospin-polarized current, and the tunnel magnetoresistance under the influence of external electric field, magnetic exchange field, and photo irradiation. However, there is more work to be done to control the unique properties of silicene in order to utilize this two-dimensional material towards spintronics and related topics, since there is only one known silicene-based device experimentally demonstrated [37], while few ideas are proposed theoretically [120, 121].

One area is the interplay between the photon and the band structure of silicene. In Chapter 6 we discovered that the external electric fields and chemical potential may have a significant impact on electron scattering at a certain light frequency, when the strength of electric fields and chemical potential reaches a certain level. The mechanism of this characteristics may need further investigation. Furthermore, we predict that both SP and VP behave in the almost exactly same manner when the chemical potential is $\mu = 0$ meV and $\mu = 2.5$ meV. However, SP shows less dependency on light frequency and VP stays almost unchanged when μ increases to 5.0 meV and 7.5 meV. Further investigations may be required to reveal the mechanism.

Another area that more investigation is necessary is in the realization of silicene devices. One challenge facing this goal is the instability of the pristine silicene layer in the air atmosphere [122]. Therefore, the interaction with substrates and the quality of silicene layer grown on substrates play important roles on the properties of silicene layer and silicene devices. Currently, the

properties of silicene grown on some substrates, such as Ag(111), ZrB_2, and Ir have been investigated, but we still need to look further to find other substrates and growth method that can provide silicene layers with higher quality and lower cost [123]. In addition, there are other properties of silicene that has not been thoroughly investigated, such as multi-layer silicene, thermal effects, strain effects, and doping effects [124-127]. More investigations on the applications of these effects are necessary in these research areas. Another area that requires further investigation is the properties of silicene as a topological insulator, and other topological phases [128-130]. The development in spintronics, quantum computers and many new technologies might benefit from the exotic properties of topological insulator.

Regarding the methodology of research, computational methods have gained the popularity, and the community has become larger in silicene and two-dimensional materials research. One reason is the availability of inexpensive and more powerful computers, as well as smarter software and more accurate models [131, 132]. Another reason is the improved perception towards computational science due to its proved track record. Currently, density functional theory is considered to be among the most reliable methods for condensed matter research with plenty of software, such as Vienna Ab initio Simulation Package (VASP), Quantum Espresso, CASTEP, and SIESTA. Therefore, computational methods could be a tool to help us have better understanding in silicene and other two-dimensional materials, in addition to theoretical analysis. Using both computational and theoretical methods will allow us to be more nimble and move faster in other two-dimensional materials research.

Bibliography

[1] T. Skotnicki, et al., "Innovative materials, devices, and CMOS technologies for low-power mobile multimedia," *IEEE Transactions on Electron Devices*, vol. 55, pp. 96-130, 2008.

[2] K. Kim, "Silicon technologies and solutions for the data-driven world," *IEEE International Solid-State Circuits Conference (ISSCC) Digest of Technical Papers*, pp. 8-14, 2015.

[3] G. E. Moore, "Cramming more components onto integrated circuits," *Electronics*, vol. 38, pp. 114-117, 1965.

[4] M. Waldrop, "More than Moore," *Nature*, vol. 530, pp. 144-147, 2016.

[5] X. Huang, et al., "Sub 50-nm FinFET: PMOS," *International Electron Devices Meeting Technical Digest*, pp. 67-70, 1999.

[6] N. Singh, et al., "High-Performance fully depleted silicon nanowire (diameter ≤ 5 nm) gate-all-around CMOS devices," *IEEE Electron Device Letters*, vol. 27, pp. 383-386, 2006.

[7] R. S. Chau, "Integrated CMOS tri-gate transistors: Paving the way to future technology generations," *Technology@Intel Magazine*, pp.1-7, 2006.

[8] G. K. Celler and Sorin Cristoloveanu, "Frontiers of silicon-on-insulator," *Journal of Applied Physics*, vol. 93, pp. 4955-4978, 2003.

[9] Y. Sun, et al., "Physics of strain effects in semiconductors and metal-oxide-semiconductor field-effect transistors," *Journal of Applied Physics*, vol.101, pp.104503, 2007.

[10] R. Chau "High-k /metal–gate stack and its MOSFET characteristics," *IEEE Electron Device Letters*, vol. 25, pp. 408-410, 2004.

[11] S. D. Bader and S. S. P. Parkin, "Spintronics," *Annual Review of Condensed Matter Physics*, vol. 1, pp. 71-88, 2010.

[12] K. L. Wang, et al., "Electric-field control of spin-orbit interaction for low-power spintronics," *Proceedings of the IEEE*, vol. 104, pp. 1974-2008, 2016.

[13] T.O. Wehling, A.M. Black-Schaffer, and A.V. Balatsky, "Dirac materials," *Advances in Physics*, vol. 63, pp. 1-76, 2014.

[14] M. Z. Hasan and J. E. Moore, "Three-dimensional topological insulators," *Annual Review of Condensed Matter Physics*, vol. 2, pp. 55-78, 2011.

[15] J. Wang, et al., "The rare two-dimensional materials with Dirac cones," *National Science Review*, vol. 2, pp. 22-39, 2015.

[16] K. S. Novoselov, et al., "Electric field effect in atomically thin carbon films," *Science*, vol. 306, pp. 666-669, 2004.

[17] P. Vogt, et al., "Silicene: Compelling experimental evidence for graphenelike two-dimensional silicon," *Physical Review Letters*, vol. 108, pp. 155501, 2012.

[18] M. E. Davila, et al., "Germanene: a novel two-dimensional germanium allotrope akin to graphene and silicene," *New Journal of Physics*, vol. 16, pp. 095002, 2014.

[19] F. Zhu, et al., "Epitaxial growth of two-dimensional stanene," *Nature Materials*, vol. 14, pp. 1020-1025, 2015.

[20] H. Zhao, et al., "Unexpected giant-gap quantum spin Hall insulator in chemically decorated plumbene monolayer," *Scientific Reports*, vol. 6, pp. 20152, 2016.

[21] G. Miert and C. M. Smith, "Dirac cones beyond the honeycomb lattice: A symmetry-based approach," *Physical Review B*, vol. 93, pp. 035401, 2016.

[22] M. F. El-Kady and R. B. Kaner, "Scalable fabrication of high-power graphene micro-supercapacitors for flexible and on-chip energy storage," *Nature Communications* , vol. 4, pp. 1475, 2013.

[23] J. T. Wang, et al., "Low-temperature processed electron collection layers of graphene/TiO2 nanocomposites in thin film perovskite solar cells," *Nano Letters*, vol. 14, pp. 724–730, 2014.

[24] S. Zhu, et al., "Graphene based piezoresistive pressure sensor," *Applied Physics Letters*, vol. 102, pp. 161904, 2013.

[25] Y. G. Semenov, K. W. Kim, and J. M. Zavada, "Spin field effect transistor with a graphene channel," *Applied Physics Letters*, vol. 91, pp. 153105, 2007.

[26] E. W. Hill, et al., "Graphene spin valve devices," *IEEE Transactions on Magnetics*, vol. 42, pp. 2694-2696, 2006.

[27] Y. Song and G. Dai, "Spin filter and spin valve in ferromagnetic graphene," *Applied Physics Letters*, vol. 106, pp. 223104, 2015.

[28] C. Chen, et al., "Graphene mechanical oscillators with tunable frequency," *Nature Nanotechnology*, vol. 8, pp. 923–927, 2013.

[29] W. Han, et al., "Graphene spintronics," *Nature Nanotechnology*, vol. 9, pp. 794–807, 2014.

[30] P. A. Denis, C. P. Huelmo, and A. S. Martins, "Band gap opening in dual-doped monolayer graphene," *The Journal of Physical Chemistry C*, vol. 120, pp. 7103–7112, 2016.

[31] J. Son, et al., "Hydrogenated monolayer graphene with reversible and tunable wide band gap and its field-effect transistor," *Nature Communications*, vol. 7, pp. 13261, 2016.

[32] W. Yang-Yang, et al., "Silicene spintronics - A concise review," *Chinese Physics B*, vol. 24, pp. 087201, 2015.

[33] Y. Kato, et al., "Coherent spin manipulation without magnetic fields in strained semiconductors," *Nature*, vol. 427, pp. 50-53, 2004.

[34] M. Ezawa, "Spin valleytronics in silicene: Quantum spin Hall–quantum anomalous Hall insulators and single-valley semimetals," *Physical Review B*, vol. 87, pp. 155415, 2013.

[35] P. Vogt, et al., "Silicene: compelling experimental evidence for graphenelike two-dimensional silicon," *Physical Review Letters*, vol. 108, pp. 155501, 2012.

[36] G.L. Lay, et al., "Silicene: silicon conquers the 2D world," *Europhysics News*, vol. 47, pp. 17-21, 2016.

[37] L. Tao, et al., "Silicene field-effect transistors operating at room temperature," *Nature Nanotechnology*, vol. 10, pp. 227-231, 2015.

[38] J. Zhao, et al., "Rise of silicene: A competitive 2D material," *Progress in Materials Science*, vol. 83, pp. 24–151, 2016.

[39] K. Takeda and K. Shiraishi, "Theoretical possibility of stage corrugation in Si and Ge analogs of graphite," *Physical Review B*, vol. 50, pp. 14916-14922, 1994.

[40] R. Friedlein and Y. Y. Takamura, "Electronic properties of epitaxial silicene on diboride thin films," *Journal of Physics: Condensed Matter*, vol. 27, pp. 203201, 2015.

[41] E. F. Sheka, "Why sp2-like nanosilicons should not form: insight from quantum chemistry," *International Journal of Quantum Chemistry*, vol. 113, pp. 612–618, 2013.

[42] E. Cinquanta, "Getting through the nature of silicene: An sp^2−sp^3 two-dimensional silicon nanosheet," *The Journal of Physical Chemistry C*, vol. 117, pp. 16719–16724, 2013.

[43] S. Cahangirov, "Two- and one-dimensional honeycomb structures of silicon and germanium," *Physical Review Letters*, vol. 102, pp. 236804, 2009.

[44] H. Liu, J. Gao, and J. Zhao, "Silicene on substrates: interaction mechanism and growth behavior," *Journal of Physics: Conference Series*, vol. 491, pp. 012007, 2014.

[45] M. Ezawa, "Monolayer topological insulators: silicene, germanene, and stanene," *Journal of the Physical Society of Japan*, vol. 84, pp. 121003-121013, 2015.

[46] M. Z. Hasan and C. L. Kane, "Colloquium: topological insulators," *Review of Modern Physics*, vol. 82, pp. 3045, 2010.

[47] C.L. Kane, E.J. Mele, "Quantum spin Hall effect in graphene," *Physical Review Letters*, vol. 95, pp. 226801, 2005.

[48] X. L. Qi and S. C. Zhang, "The quantum spin Hall effect and topological insulators," *Physics Today*, vol. 63, pp. 33-38, 2010.

[49] M. Ezawa, "Quantum Hall effects in silicene," *Journal of the Physical Society of Japan*, vol. 81, pp. 064705-064710, 2012.

[50] K. V. Klitzing, G. Dorda, and M. Pepper, "New method for high-accuracy determination of the fine-structure constant based on quantized Hall resistance," *Physical Review Letters*, vol. 45, pp. 494-497, 1980.

[51] L. Fu and C. L. Kane, "Topological insulators with inversion symmetry," *Physical Review B*, vol. 76, pp. 045302, 2007.

[52] Y. K. Kato, et al., "Observation of the spin Hall effect in semiconductors," *Science*, vol. 306, pp. 1910-1913, 2004.

[53] M. I. Dyakonov and V. I. Perel, "Current-induced spin orientation of electrons in semiconductors" *Physics Letters A*, vol. 35, pp. 459-460, 1971.

[54] M. Ezawa, "A topological insulator and helical zero mode in silicene under an inhomogeneous electric field," *New Journal of Physics*, vol. 14, pp. 033003, 2012.

[55] C.-C. Liu, W. Feng, and Y. Yao, "Quantum spin hall effect in silicene and two-dimensional germanium," *Physical Review Letters*, vol. 107, pp. 076802, 2011.

[56] T. Yokoyama, "Spin and valley transports in junctions of Dirac fermions," *New Journal of Physics*, vol. 16, pp. 085005, 2014.

[57] D. Xiao, et al., "Coupled spin and valley physics in monolayers of MoS_2 and other group-VI dichalcogenides," *Physical Review Letters*, vol. 108, pp. 196802, 2012.

[58] M. Ezawa, "Valley-polarized metals and quantum anomalous Hall effect in silicene," *Physical Review Letters*, vol. 109, pp. 055502, 2012.

[59] J.A. Yan, et al., "Electron-phonon coupling in two-dimensional silicene and germanene," *Physical Review B*, vol. 88, pp. 121403, 2013.

[60] H. Chang, et al., "Probing the topological phase transition via density oscillations in silicene and germanene," *Physical Review B*, vol. 89, pp. 201411(R), 2014.

[61] T. Yokoyama, "Spin and valley transports in junctions of Dirac fermions," *New Journal of Physics*, vol. 16, 085005, 2014.

[62] T. Yokoyama, "Controllable valley and spin transport in ferromagnetic silicene junctions," *Physical Review B*, vol. 87, pp. 241409(R), 2013.

[63] V. Vargiamidis and P. Vasilopoulos, "Electric- and exchange-field controlled transport through silicene barriers: Conductance gap and near-perfect spin polarization," *Applied Physics Letters*, vol. 105, pp. 223105, 2014.

[64] X. Qiu, et al., "Valley-dependent electron transport in ferromagnetic / normal / ferromagnetic silicene junction," *Current Applied Physics*, vol. 15, pp. 722-726, 2015.

[65] K. Zberecki, R. Swirkowicz, and J. Barnas, "Thermoelectric properties of zigzag silicene nanoribbons doped with Co impurity atoms," *Journal of Magnetism and Magnetic Materials*, vol. 393, pp. 305, 2015.

[66] B. Soodchomshom, "Perfect spin-valley filter controlled by electric field in ferromagnetic silicene," *Journal of Applied Physics*, vol. 115, pp. 023706, 2014.

[67] X.Q. Wu and H. Meng, "Gate-tunable valley-spin filtering in silicene with magnetic barrier," *Journal of Applied Physics*, vol. 117, pp. 203903, 2015.

[68] W. F. Tsai, et al., "Gated silicene as a tunable source of nearly 100% spin-polarized electrons," *Nature Communications*, vol. 4, pp. 1500, 2013.

[69] Y. Wang and Y. Lou, "Controllable spin transport in dual-gated silicene," *Physics Letters A*, vol. 378, pp. 2627, 2014.

[70] B. Van Duppen, P. Vasilopoulos, and F. M. Peeters, "Spin and valley polarization of plasmons in silicene due to external fields," *Physical Review B*, vol. 90, pp. 035142, 2014.

[71] P. Chantngarm, K. Yamada, B. Soodchomshom, "Lattice-pseudospin and spin-valley polarizations in dual ferromagnetic-gated silicene junction," *Superlattices and Microstructures*, vol. 94, pp. 13-24, 2016.

[72] T. Kitagawa, et al., "Transport properties of nonequilibrium systems under the application of light: Photoinduced quantum Hall insulators without Landau levels," *Physical Review B*, vol. 84, pp. 235108, 2011.

[73] M. Ezawa, "Photoinduced Topological Phase Transition and a Single Dirac-Cone State in Silicene," *Physical Review Letters*, vol. 110, pp. 026603, 2013.

[74] M. Ezawa, "Photo-induced topological superconductor in silicene, germanene, and stanene," *Journal of Superconductivity and Novel Magnetism*, vol. 28, pp. 1249–1253, 2015.

[75] Y. Mohammadi and B. A. Nia, "Controllable photo-induced spin and valley filtering in silicene," *Superlattices and Microstructures*, vol. 96, pp. 259-266, 2016.

[76] L. B. Ho and T. N. Lan, "Photoenhanced spin/valley polarization and tunneling magnetoresistance in ferromagnetic-normal-ferromagnetic silicene junction," *Journal of Physics D: Applied Physics*, vol. 49, pp. 375106, 2016.

[77] A. Lopez, et al., "Photoinduced pseudospin effects in silicene beyond the off-resonant condition," *Physical Review B*, vol. 91, pp. 125105, 2015.

[78] M. Houssa, "Electronic properties of hydrogenated silicene and germanene," *Applied Physics Letters*, vol. 98, pp. 223107, 2011.

[79] R. Zhang, et al., "Silicane as an inert substrate of silicene: A promising candidate for FET," *The Journal of Physical Chemistry C*, vol. 118, pp. 25278-25283, 2014.

[80] C. Zhang and S. Yan, "First-principles study of ferromagnetism in two-dimensional silicene with hydrogenation," *The Journal of Physical Chemistry C*, vol. 116, pp. 4163-4166, 2012.

[81] P. Vogt, et al., "Synthesis and electrical conductivity of multilayer silicene," *Applied Physics Letters*, vol. 104, pp. 021602, 2014.

[82] H. Tsai, et al., "Synthesis of nonepitaxial multilayer silicene assisted by ion implantation," *Nanoscale*, vol. 8, pp. 9488-9492, 2016.

[83] C. Kamal, et al., "Silicene beyond mono-layers—different stacking configurations and their properties," *Journal of Physics: Condensed Matter*, vol. 25, pp. 085508, 2013.

[84] Y. Wang and Y. Ding, "Strain-induced self-doping in silicene and germanene from first-principles," *Solid State Communications*, vol. 155, pp. 6-11, 2013.

[85] D. Harper, C. Wooff, and D. Hodgkinson, *A Guide to computer algebra systems*, John Wiley & Sons Inc, 1991.

[86] W. Shen, *An Introduction to numerical computation*, World Scientific Publishing Company, 2015.

[87] R. H. Landau, J. Paez, and C. C. Bordeianu, *A survey of computational physics: Introductory computational science*, Princeton University Press, 2008.

[88] K. Capelle, "A bird's-eye view of density-functional theory," *Brazilian Journal of Physics*, vol. 36, pp. 1318-1343, 2006.

[89] K. Ohno, K. Esfarjani, Y. Kawazoe, *Computational materials science: From ab initio to Monte Carlo methods*, Springer, 2000.

[90] J. C. Slater and G. F. Koster, "Simplified LCAO method for the periodic potential problem," *Physical Review*, vol. 94, pp. 1498-1524, 1954.

[91] C. Kittel, *Introduction to solid state physics*, Wiley, 2004.

[92] A. V. Gert, M. O. Nestoklon, and I. N. Yassievich, "Band structure of silicene in the tight binding approximation," *Journal of Experimental and Theoretical Physics*, vol. 12, pp. 115-121, 2015.

[93] L. Susskind, and A. Friedman, *Quantum mechanics: The theoretical minimum*. Basic Books, 2014.

[94] D. Xiao, W. Yao, and Q. Niu, "Valley-contrasting physics in graphene: Magnetic moment and topological transport," *Physical Review Letters*, vol. 99, pp. 236809, 2007.

[95] P. Gosselin, "Berry curvature in graphene: A new approach," *The European Physical Journal C*, vol. 59, pp. 883-889, 2009.

[96] M. V. Berry, "Quantal phase factors accompanying adiabatic changes," *Proceedings of the Royal Society of London A*, vol. 392, pp. 45-57, 1984.

[97] K. Y. Bliokh, Y .P. Bliokh, "Spin gauge fields: From Berry phase to topological spin transport and Hall effects," *Annals of Physics*, vol. 319, pp. 13–47, 2005.

[98] K. S. Novoselov, "Graphene: The magic of flat carbon," *ECS Transactions*, vol. 19, pp. 3-7, 2009.

[99] X. T. An, et al., "Spin-polarized current induced by a local exchange field in a silicene nanoribbon," *New Journal of Physics*, vol. 14, pp. 083039, 2012.

[100] H. Haugen, D. H. Hernando, and A. Brataas, "Spin transport in proximity-induced ferromagnetic graphene," *Physical Review B*, vol. 77, pp. 115406 , 2008.

[101] A. G. Swartz, et al., "Integration of the ferromagnetic insulator EuO onto graphene," *ACS Nano*, vol. 6, pp. 10063-10069, 2012.

[102] J. D. Hoffman, S. Frankel, *Numerical Methods for Engineers and Scientists*, CRC Press, 2001.

[103] M. Ezawa, "Topological phase transition and electrically tunable diamagnetism in silicene," *The European Physical Journal B*, vol.85, pp. 363, 2012.

[104] C. C. Liu, H. Jiang, and Y. Yao, "Low-energy effective Hamiltonian involving spin-orbit coupling in silicene and two-dimensional germanium and tin," *Physical Review B*, vol. 84, pp. 195430, 2011.

[105] K. S. Novoselov, et al., "Two-dimensional gas of massless Dirac fermions in graphene," *Nature*, vol. 438, pp. 197, 2005.

[106] R. Landauer, "Spatial variation of currents and fields due to localized scatterers in metallic conduction," *IBM Journal of Research and Development*, vol. 1, pp. 223-231, 1957.

[107] B. Soodchomshom, "Valley-dependent tunneling in a monolayer gapped graphene without strain," *Physica E*, vol. 44, pp. 1617-1622, 2012.

[108] L. Majidi and M. Zareyan, "Pseudospin polarized quantum transport in monolayer graphene," *Physical Review B*, vol. 83, pp. 115422, 2011.

[109] G. P. Konnen, *Polarized Light in Nature*, Cambridge University Press, 1985.

[110] Dave3457 (Own work) [Public domain], via Wikimedia Commons.

[111] U. D. Giovannini, H. Hubener, and A. Rubio, "Monitoring electron-photon dressing in WSe$_2$," *Nano Letters*, vol. 16, pp. 7993–7998, 2016.

[112] F. H. M. Faisal and J. Z. Kaminski, "Floquet-Bloch theory of high-harmonic generation in periodic structures," *Physical Review A*, vol. 56, pp. 748-762, 1997.

[113] J. C. Slater and G. F. Koster, "Simplified LCAO method for the periodic potential problem," *Physical Review*, vol. 94, pp. 1498-1524, 1954.

[114] W. A. Harrison, *Electronic structure and the properties of solids: The physics of the chemical bond*, Dover Publications, 1989.

[115] M. Finnis, *Interatomic forces in condensed matter*, Oxford University Press, 2010.

[116] D. A. Papaconstantopoulos and M. J. Mehl, "The Slater-Koster tight-binding method: a computationally efficient and accurate approach," *Journal of Physics: Condensed Matter*, vol. 15, pp.R413-R440, 2003.

[117] M. Elstner, et al., "Self-consistent-charge density-functional tight-binding method for simulations of complex materials properties," *Physical Review B*, vol. 58, pp. 7260-7268, 1998.

[118] L. A. Agapito, et al., "Accurate tight-binding Hamiltonians for two-dimensional and layered materials," *Physical Review B*, vol. 93, pp. 125137, 2016.

[119] R. Cote and M. Barrette, "Validity of the two-component model of bilayer and trilayer graphene in a magnetic field," *Physical Review B*, vol. 88, pp. 245445, 2013.

[120] C. Nunez, et al., "Silicene-based spin-filter device: impact of random vacancies," *2D Materials*, vol. 3, pp. 025006, 2016.

[114] R. G. Amorim and R. H. Scheicher, "Silicene as a new potential DNA sequencing device," *Nanotechnology*, vol. 26, pp. 154002, 2015.

[115] G. Liu, et al., "Comparison of the stability of free-standing silicene and hydrogenated silicene in oxygen: a first principles investigation," *Journal of Physics: Condensed Matter*, vol. 26, pp. 355007, 2014.

[116] J. Sone, et al., "Epitaxial growth of silicene on ultra-thin Ag(111) films," *New Journal of Physics*, vol. 16, pp. 095004, 2014.

[117] P. D. Padova, et al., "Multilayer silicene: clear evidence," *2D Materials*, vol. 3, pp. 031011, 2016.

[118] B. Liu, et al., "Thermal conductivity of silicene nanosheets and the effect of isotopic doping," *Journal of Physics D: Applied Physics*, vol. 47, pp. 165301, 2014.

[119] C. Lian and J. Ni, "Strain induced phase transitions in silicene bilayers: a first principles and tight-binding study," *AIP Advances*, vol. 3, pp. 052102, 2013.

[120] Q. X. Pei, "Tuning the thermal conductivity of silicene with tensile strain and isotopic doping: A molecular dynamics study," *Journal of Applied Physics*, vol. 114, pp. 033526, 2013.

[121] M. Tahir and U. Schwingenschlogl, "Valley polarized quantum Hall effect and topological insulator phase transitions in silicene," *Scientific Reports*, vol. 3, pp. 1075, 2013.

[122] L. Kou, et al., "Encapsulated silicene: A robust large-gap topological insulator," *ACS Applied Materials and Interfaces*, vol. 7, pp. 19226–19233, 2015.

[123] Y. Xu, X. Zhou, and G. Jin, "Detecting topological phases in silicene by anomalous Nernst effect," *Applied Physics Letters*, vol. 108, pp. 203104, 2016.

[124] A. B. Shiflet and G. W. Shiflet, *Introduction to computational science: Modeling and simulation for the sciences*, Princeton University Press, 2014.

[132] U. Rude, "Research and education in computational science and engineering," *arXiv:1610.02608 [cs.CE]*, 2016.

Acknowledgments

List of Publications

Chapter 4   P. Chantngarm, K. Yamada, and B. Soodchomshom, "Lattice-pseudospin and spin-valley polarizations in dual ferromagnetic-gated silicene junction," *Superlattices and Microstructures*, vol. 94, pp. 13-24, 2016.

Chapter 5   P. Chantngarm and K. Yamada, "Effects of polarized light irradiation on double-ferromagnetic-gate silicene junction," in *Proceedings of The 14th International Conference ECTI-CON 2017, Phuket, Thailand, 27-30 June 2017*, pp. 72-75.

Chapter 6   P. Chantngarm, K. Yamada, and B. Soodchomshom, "Polarized-photon frequency filter in double-ferromagnetic barrier silicene junction," *Journal of Magnetism and Magnetic Materials*, vol. 429, pp. 16-22, 2017.